

Measurement of non-prompt D0-meson elliptic flow in Pb-Pb collisions at $\sqrt{s_{NN}}=5.02$ TeV

(ALICE Collaboration) Acharya, S.; ...; Erhardt, Filip; ...; Gotovac, Sven; ...; Karatović, David; ...; Lončar, Petra; ...; ...

Source / Izvornik: **The European Physical Journal C, 2023, 83**

Journal article, Published version

Rad u časopisu, Objavljena verzija rada (izdavačev PDF)

<https://doi.org/10.1140/epjc/s10052-023-12259-3>

Permanent link / Trajna poveznica: <https://urn.nsk.hr/urn:nbn:hr:217:117965>

Rights / Prava: [Attribution 4.0 International](#)/[Imenovanje 4.0 međunarodna](#)

Download date / Datum preuzimanja: **2024-09-18**



Repository / Repozitorij:

[Repository of the Faculty of Science - University of Zagreb](#)





Measurement of non-prompt D^0 -meson elliptic flow in Pb–Pb collisions at $\sqrt{s_{NN}} = 5.02$ TeV

ALICE Collaboration*

CERN, 1211 Geneva 23, Switzerland

Received: 8 September 2023 / Accepted: 15 November 2023 / Published online: 11 December 2023
© CERN for the benefit of The ALICE Collaboration 2023

Abstract The elliptic flow (v_2) of D^0 mesons from beauty-hadron decays (non-prompt D^0) was measured in midcentral (30–50%) Pb–Pb collisions at a centre-of-mass energy per nucleon pair $\sqrt{s_{NN}} = 5.02$ TeV with the ALICE detector at the LHC. The D^0 mesons were reconstructed at midrapidity ($|y| < 0.8$) from their hadronic decay $D^0 \rightarrow K^- \pi^+$, in the transverse momentum interval $2 < p_T < 12$ GeV/ c . The result indicates a positive v_2 for non-prompt D^0 mesons with a significance of 2.7σ . The non-prompt D^0 -meson v_2 is lower than that of prompt non-strange D mesons with 3.2σ significance in $2 < p_T < 8$ GeV/ c , and compatible with the v_2 of beauty-decay electrons. Theoretical calculations of beauty-quark transport in a hydrodynamically expanding medium describe the measurement within uncertainties.

1 Introduction

A phase of matter made of deconfined quarks and gluons, called the quark-gluon plasma (QGP), is created in ultrarelativistic heavy-ion collisions, as supported by several measurements at the SPS, RHIC, and LHC particle accelerators [1–9]. The QGP formed in such extreme conditions is considered to be a nearly perfect fluid [10]. Heavy quarks (charm and beauty), mostly produced via hard partonic scattering processes on a timescale shorter than the QGP formation time [11, 12], are effective probes of the properties and dynamics of the QGP. They interact with the medium constituents, losing energy via radiative and collisional processes [13]. The significant suppression of charm- and beauty-hadron production yields at intermediate and high transverse momentum ($p_T > 6$ GeV/ c) observed in heavy-ion collisions at both RHIC [14–18] and LHC [19–33], compared to appropriately scaled yields from proton–proton (pp) collisions, indicates a substantial energy loss of heavy quarks in the QGP.

The azimuthal anisotropy in momentum space of final-state hadrons acts as an additional observable to probe the properties of the QGP. In non-central nucleus–nucleus collisions,

the spatial anisotropy in the initial matter distribution due to the asymmetry of the nuclear overlap region is transferred to the final-state particle momentum distribution via multiple collisions, a phenomenon referred to as anisotropic flow [34, 35]. The anisotropic flow is quantified by the harmonic coefficients $v_n = \langle \cos[n(\varphi - \Psi_n)] \rangle$ of the Fourier expansion of the particle azimuthal angle (φ) relative to the collision symmetry planes with angles Ψ_n for the n th harmonic. The second harmonic, v_2 , also known as elliptic flow, is the largest coefficient in non-central heavy-ion collisions. At low p_T ($p_T < 6$ GeV/ c), the heavy-flavour v_2 can help to quantify the extent to which charm and beauty quarks participate in the collective expansion of the medium [36] and the fraction of heavy quarks hadronising via recombination with light quarks in the QGP medium in the intermediate p_T region ($6 < p_T < 10$ GeV/ c) [37, 38]. In addition, at high p_T ($p_T > 10$ GeV/ c), the v_2 of heavy-flavour hadrons can constrain the path-length dependence of energy loss in the medium for heavy quarks [39, 40].

D mesons and charm-hadron decay leptons show a positive v_2 in nucleus–nucleus collisions at both RHIC [14, 41–43] and LHC [44–53] energies. The comparison of experimental measurements with theoretical models indicates that charm quarks participate in the collective expansion of the medium, and both collisional processes and the hadronisation of charm quarks via coalescence with light quarks are important to describe the observed elliptic flow [54–63]. In particular, the D-meson v_2 has a magnitude similar to the v_2 of charged pions for $3 < p_T < 6$ GeV/ c , suggesting that low- p_T charm quarks have a relaxation time comparable to the QGP lifetime [64]. Due to their higher mass, beauty quarks are unlikely to reach thermalisation in the medium, therefore their azimuthal anisotropy can give further insight into the interactions of heavy quarks with the medium [65–68]. The experimental information is still poor for the beauty-hadron v_2 at low momentum. The elliptic flow of J/ψ mesons originating from beauty-hadron decays (non-prompt) measured by the CMS and ATLAS Collaborations is consistent with zero within large uncertainties for $p_T > 3$ GeV/ c [69, 70].

* e-mail: alice-publications@cern.ch

The v_2 of leptons from beauty-hadron decays measured by ALICE and ATLAS is found to be positive [71, 72]. However, due to the small lepton masses, correlations between the kinematic variables (p_T and direction) of the beauty hadrons and the decay leptons are broad. This is improved when choosing a decay into a heavier particle. A measurement of the non-prompt D^0 -meson v_2 has been recently submitted for publication by CMS [73].

In this letter, the measurement of the non-prompt D^0 -meson v_2 at midrapidity ($|y| < 0.8$) in Pb–Pb collisions at a centre-of-mass energy per nucleon pair $\sqrt{s_{NN}} = 5.02$ TeV with the ALICE detector is reported. The D^0 -meson v_2 is measured with the Scalar Product (SP) method [74, 75] in midcentral collisions (30–50% centrality class). The non-prompt D^0 -meson v_2 is extracted and compared with previous measurements of the prompt non-strange D-meson v_2 (average of D^0 , D^+ , and D^{*+}) and the v_2 of electrons from beauty-hadron decays, as well as with theoretical models based on beauty-quark transport in the QGP.

2 Experimental apparatus and data analysis

A description of the ALICE detector and its performance can be found in Refs. [9, 76, 77]. The main detectors used for this analysis are the Inner Tracking System (ITS) [78] for track and vertex reconstruction, the Time Projection Chamber (TPC) [79] for track reconstruction and particle identification (PID) via the measurement of the specific energy loss, and the Time-Of-Flight (TOF) [80] detector for PID via the measurement of the particle flight time from the interaction point to the detector. These detectors are located inside a large solenoidal magnet providing a magnetic field of up to 0.5 T parallel to the LHC beam direction and cover the pseudorapidity interval $|\eta| < 0.9$. A minimum-bias interaction trigger was used, requiring coincident signals in the V0A and V0C detectors [81], two scintillator arrays covering the full azimuth in the pseudorapidity intervals $2.8 < \eta < 5.1$ (V0A) and $-3.7 < \eta < -1.7$ (V0C). An online selection based on the V0 signal amplitudes was also applied in order to enhance the sample of midcentral collisions as an additional trigger class. Background events from beam–gas interactions were rejected offline using the timing information provided by the V0 and the neutron Zero-Degree Calorimeter (ZDC) [82]. Events used in the analysis were required to have a primary vertex reconstructed within ± 10 cm from the nominal interaction point along the beam axis. Centrality intervals for events were defined in terms of percentiles of the hadronic Pb–Pb cross section based on the signal amplitude of the V0 detectors [83]. After the aforementioned selections, a sample of about 85×10^6 events in the 30–50% centrality class was utilised for further analysis, corresponding to an integrated luminosity of $\mathcal{L}_{\text{int}} \simeq 56 \mu\text{b}^{-1}$ [84].

The D^0 mesons and their charge conjugates were reconstructed via the hadronic decay channel $D^0 \rightarrow K^- \pi^+$ with branching ratio $\text{BR} = (3.947 \pm 0.030)\%$ [85]. The D^0 -meson candidates were selected combining pairs of tracks with opposite charge signs, each with $p_T > 0.3$ GeV/ c and $|\eta| < 0.8$. The selection criteria require at least 70 (out of 159) associated space points in the TPC, a minimum of two (out of six) measured clusters in the ITS, with at least one in either of the two innermost layers, and a fit quality $\chi^2/\text{ndf} < 1.25$ in the TPC. These track selection criteria reduce the D^0 -meson acceptance in rapidity, which falls steeply to zero for $|y| > 0.5$ at low p_T and for $|y| > 0.8$ for $p_T > 5$ GeV/ c . Thus, a fiducial acceptance selection $|y| < y_{\text{fid}}(p_T)$ was applied to grant a uniform acceptance inside the rapidity range considered. The $y_{\text{fid}}(p_T)$ value was defined as a second-order polynomial function, increasing from 0.5 to 0.8 in $0 < p_T < 5$ GeV/ c , and as a constant term, $y_{\text{fid}} = 0.8$, for $p_T > 5$ GeV/ c .

A machine-learning approach with multi-class classification based on Boosted Decision Trees (BDT) was adopted to simultaneously suppress the large combinatorial background and separate the contributions of prompt and non-prompt D^0 mesons. The implementation of the BDT algorithm provided by the XGBoost [86] library was employed. Samples of prompt and non-prompt D^0 mesons for the BDT training were obtained from Monte Carlo (MC) samples, which simulated the Pb–Pb events at $\sqrt{s_{NN}} = 5.02$ TeV with the HIJING v1.383 generator [87]. Additional $c\bar{c}$ or $b\bar{b}$ quark pairs were injected in each simulated event using the PYTHIA 8.243 event generator [88, 89] (Monash 2013 tune [90]) to enrich the MC sample of prompt and non-prompt D^0 -meson signals. The generated particles were transported through the experimental apparatus using the GEANT3 transport package [91]. Samples for the combinatorial background were obtained from candidates in the sideband region in the data, i.e. $5\sigma < |\Delta M| < 9\sigma$ in the invariant mass distribution, where ΔM is the difference between the invariant mass and the mean of signal distribution, and σ is the invariant-mass resolution. Before the training, loose selections on kinematic and topological variables were applied to the D^0 -meson candidates to reduce the computation time. The training variables provided to the BDTs were mainly based on the displacement of the D^0 decay vertex from the primary vertex of the collision. These included the impact parameter of the D^0 -meson daughter tracks, the distance between the D^0 -meson decay vertex and the primary vertex, and the cosine of the pointing angle between the D^0 -meson candidate line of flight (the vector connecting the primary and secondary vertices) and its reconstructed momentum vector, as well as the PID information of the decay tracks. A detailed description of the training procedure is reported in Ref. [92]. Independent BDTs were trained in the different p_T intervals of the analysis. Subsequently, the BDTs were applied to the experimental

data sample to obtain the BDT scores related to the candidate probability to be a non-prompt D^0 meson or to belong to the combinatorial background. Selections were applied on the scores to reduce the large combinatorial background and to obtain different fractions of non-prompt D^0 candidates ($f_{\text{non-prompt}}$). The D^0 -meson v_2 coefficient was measured with the Scalar Product (SP) method [74, 75, 93],

$$v_2\{\text{SP}\} = \left\langle \left\langle \mathbf{u}_2 \cdot \frac{\mathbf{Q}_2^{\text{VOC}*}}{M^{\text{VOC}}} \right\rangle \right\rangle / \sqrt{\frac{\left\langle \frac{\mathbf{Q}_2^{\text{VOC}}}{M^{\text{VOC}}} \cdot \frac{\mathbf{Q}_2^{\text{V0A}*}}{M^{\text{V0A}}} \right\rangle \left\langle \frac{\mathbf{Q}_2^{\text{VOC}}}{M^{\text{VOC}}} \cdot \frac{\mathbf{Q}_2^{\text{TPC}*}}{M^{\text{TPC}}} \right\rangle}{\left\langle \frac{\mathbf{Q}_2^{\text{V0A}}}{M^{\text{V0A}}} \cdot \frac{\mathbf{Q}_2^{\text{TPC}*}}{M^{\text{TPC}}} \right\rangle}}$$

$$= \left\langle \left\langle \mathbf{u}_2 \cdot \frac{\mathbf{Q}_2^{\text{VOC}*}}{M^{\text{VOC}}} \right\rangle \right\rangle / R_2, \tag{1}$$

where $\mathbf{u}_2 = e^{i2\varphi_{D^0}}$ is the unit flow vector of the D^0 -meson candidate with azimuthal angle φ_{D^0} . \mathbf{Q}_2^k and M^k are the subevent 2nd harmonic flow vector and multiplicity for the subevent k , respectively. The denominator, called the resolution (R_2), is calculated with the formula introduced in Ref. [75], where the three subevents are defined by the particles measured in the VOC, V0A, and TPC detectors, respectively. For the TPC detector, the azimuthal angles of charged tracks reconstructed with $|\eta| < 0.8$ and the number of measured tracks were used to calculate the \mathbf{Q}_2 vector and M . For the V0A and VOC detectors, the \mathbf{Q}_2 vectors were calculated from the azimuthal distribution of the energy deposition in the detector scintillators and M is the sum of the amplitudes measured in each channel [52]. The \mathbf{Q}_2 vectors are recalibrated using a recentering procedure [94] to correct for effects of non-uniform acceptance. The nonflow effects are suppressed by the pseudorapidity gaps between the TPC, V0A, and VOC detectors [95]. The single bracket $\langle \rangle$ in Eq. 1 refers to an average over all the events, while the double brackets $\langle \langle \rangle \rangle$ denote the average over all particles in the considered p_T interval and all events. The R_2 is extracted as a function of the collision centrality. The centrality-integrated R_2 value is 0.0438 for the 30–50% centrality class.

The D^0 -meson v_2 cannot be measured directly using Eq. 1 since D^0 mesons cannot be identified on a particle-by-particle basis. Therefore, a simultaneous fit to the invariant-mass spectrum and the v_2 distribution as a function of the invariant mass ($M_{K\pi}$) was performed for D^0 candidates in each p_T interval, in order to measure the raw yields and the v_2 coefficients. The measured total elliptic flow coefficient, v_2^{tot} , can be written as a weighted sum of the v_2 of the D^0 -meson candidates (v_2^{sig}), and that of background (v_2^{bkg}) [96] as

$$v_2^{\text{tot}}(M_{K\pi}) = v_2^{\text{sig}} \frac{N^{\text{sig}}}{N^{\text{sig}} + N^{\text{bkg}}}(M_{K\pi}) + v_2^{\text{bkg}}(M_{K\pi}) \frac{N^{\text{bkg}}}{N^{\text{sig}} + N^{\text{bkg}}}(M_{K\pi}), \tag{2}$$

where N^{sig} and N^{bkg} are the raw signal and background yields, respectively. The fit function for the D^0 -candidate invariant-mass distribution was composed of a Gaussian term to describe the signal and an exponential distribution for the background. The contribution of signal candidates with the reflected $K-\pi$ mass assignment was taken into account with an additional term, which is small thanks to the good PID capability. It was parameterised by fitting the simulated invariant-mass distribution with a double Gaussian function. To improve the stability of the fits, the widths of the signal peaks were fixed to the values extracted from the fits of the invariant-mass distributions in the prompt enhanced sample, given the naturally larger abundance of prompt compared to non-prompt candidates. In the simultaneous fit, the v_2 parameter for the candidates with wrong $K-\pi$ mass assignment was set to be equal to v_2^{sig} , provided that the origin of these candidates are real D^0 mesons. The v_2^{sig} was measured from the fit to the v_2^{tot} distribution with the function of Eq. 2, where v_2^{bkg} is a linear as a function of $M_{K\pi}$ for $p_T > 3 \text{ GeV}/c$. For $p_T < 3 \text{ GeV}/c$, a second-order polynomial function was used to parametrise $v_2^{\text{bkg}}(M_{K\pi})$. Figure 1 shows an example of the simultaneous fit to the invariant-mass spectrum and v_2^{tot} as a function of $M_{K\pi}$ with low (left panel) and high (right panel) non-prompt D^0 -meson candidate BDT score selections in $3 < p_T < 4 \text{ GeV}/c$ in the 30–50% centrality class.

The reconstructed D^0 -meson signals are a mixture of prompt and non-prompt D^0 mesons. The v_2^{sig} is therefore a linear combination of prompt (v_2^{prompt}) and non-prompt ($v_2^{\text{non-prompt}}$) contributions, which can be expressed as

$$v_2^{\text{sig}} = (1 - f_{\text{non-prompt}})v_2^{\text{prompt}} + f_{\text{non-prompt}}v_2^{\text{non-prompt}}, \tag{3}$$

where $f_{\text{non-prompt}}$ is estimated as a function of p_T with a data-driven method, which is based on the construction of data samples with different abundances of prompt and non-prompt candidates. A set of raw yields Y_i (index i refers to a given selection on the BDT scores) can be obtained by varying the selection on the BDT score, which is related to the candidate probability to be a non-prompt D^0 meson. These raw yields are related to the corresponding acceptance times efficiency ($\text{Acc} \times \epsilon$) of prompt and non-prompt D^0 mesons according to the equation

$$(\text{Acc} \times \epsilon)_i^{\text{prompt}} N_{\text{prompt}} + (\text{Acc} \times \epsilon)_i^{\text{non-prompt}} N_{\text{non-prompt}} - Y_i = \delta_i, \tag{4}$$

where δ_i represents a residual that accounts for the equation not summing exactly to 0 due to the uncertainties on Y_i , $(\text{Acc} \times \epsilon)_i^{\text{non-prompt}}$, and $(\text{Acc} \times \epsilon)_i^{\text{prompt}}$. By applying at least two different BDT selections and extracting the yields, the corrected yields of prompt (N_{prompt}) and non-prompt ($N_{\text{non-prompt}}$) D^0 mesons can be obtained from Eq. 4 via

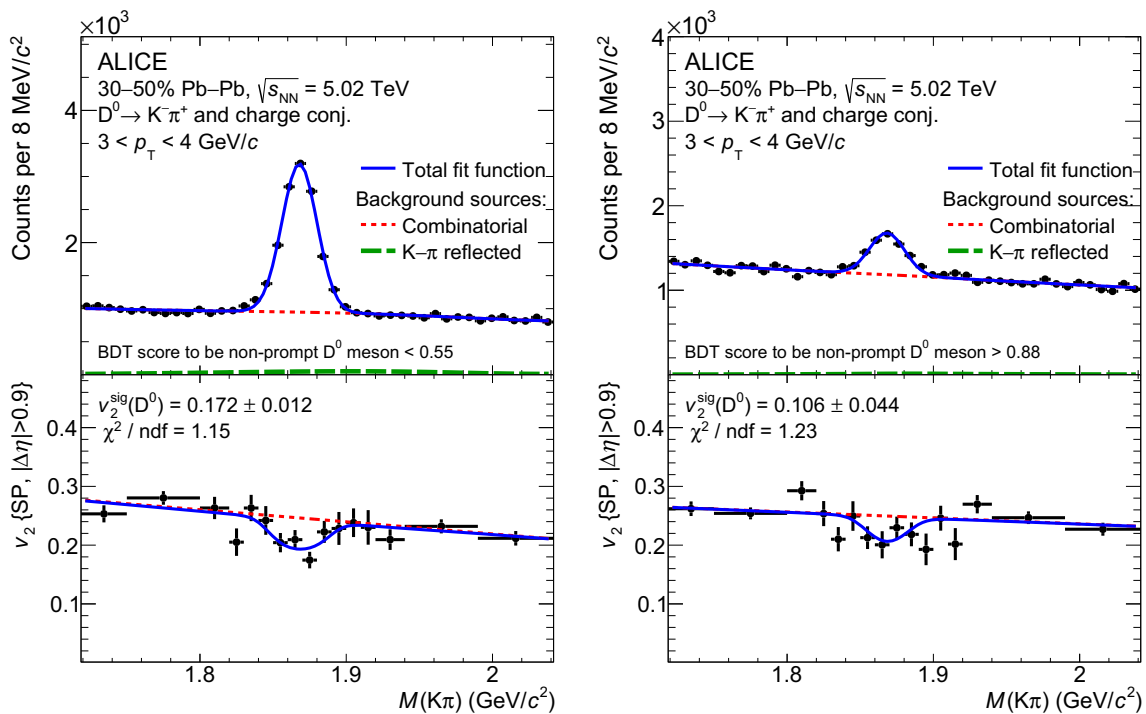


Fig. 1 Simultaneous fits of the invariant-mass distribution and $v_2^{tot}(M_{K\pi})$ of D^0 mesons in $3 < p_T < 4$ GeV/c. Left panel: Fits using D^0 -meson candidates with low probability to be a non-prompt D^0 meson. Right panel: Fits using D^0 -meson candidates with high probability to be a non-prompt D^0 meson. The corresponding BDT score

selection for the measured raw yield is reported. The blue lines, the dotted red curves, and the green solid lines represent the total fit function, the combinatorial-background fit function, and the contribution of the reflected signal, respectively

a χ^2 minimisation. More details can be found in Ref. [92]. The left panel of Fig. 2 shows an example of the raw-yield distributions as a function of the minimum non-prompt D^0 -meson BDT score threshold used in such a χ^2 -minimisation procedure in $3 < p_T < 4$ GeV/c for the 30–50% centrality class. The raw yield decreases with the increasing minimum threshold for the score to be a non-prompt D^0 meson, corresponding to an increasing non-prompt D^0 -meson fraction. The prompt and non-prompt components of the raw yields for each BDT-based selection obtained from the χ^2 -minimisation approach, $(Acc \times \epsilon)_i^{prompt} \times N_{prompt}$ and $(Acc \times \epsilon)_i^{non-prompt} \times N_{non-prompt}$, are shown in the histograms with red and blue colour, respectively, and their sum is reported by the green line. The values of $N_{non-prompt}$ and N_{prompt} can be used to estimate the non-prompt D^0 -meson fraction in the raw yield for any set of selections i using

$$f_{non-prompt}^i = \frac{(Acc \times \epsilon)_i^{non-prompt} N_{non-prompt}}{(Acc \times \epsilon)_i^{non-prompt} N_{non-prompt} + (Acc \times \epsilon)_i^{prompt} N_{prompt}} \quad (5)$$

The v_2^{sig} was determined for three or four non-overlapping intervals of BDT score to be non-prompt D^0 mesons, depending on the number of candidates in each p_T interval. The result was extrapolated to $f_{non-prompt} = 0$ and $f_{non-prompt}$

= 1 using a linear fit according to Eq. 3 in order to estimate the v_2 values for prompt and non-prompt D^0 mesons, respectively. A similar approach was adopted in Ref. [97]. The right panel of Fig. 2 shows the linear fit of v_2^{sig} as a function of $f_{non-prompt}$ in $3 < p_T < 4$ GeV/c. The blue band represents the 1σ confidence interval obtained from the linear fit, which is considered as the statistical uncertainty of the v_2^{sig} . As a crosscheck about the correlation of the statistical uncertainties on v_2^{sig} between different values of $f_{non-prompt}$, the statistical uncertainty was also calculated with the Jackknife method [98] and found to be consistent with the fit method.

3 Systematic uncertainties

Four major sources of systematic uncertainties were considered for the measurement of the non-prompt D^0 -meson v_2 : (i) the signal extraction from the invariant-mass and v_2^{tot} distributions; (ii) the non-prompt fraction estimation; (iii) the D-meson p_T shape in the simulation; and (iv) the centrality dependence of the SP denominator (R_2). All sources of systematic uncertainties were treated as uncorrelated and added in quadrature to obtain the total systematic uncertain-

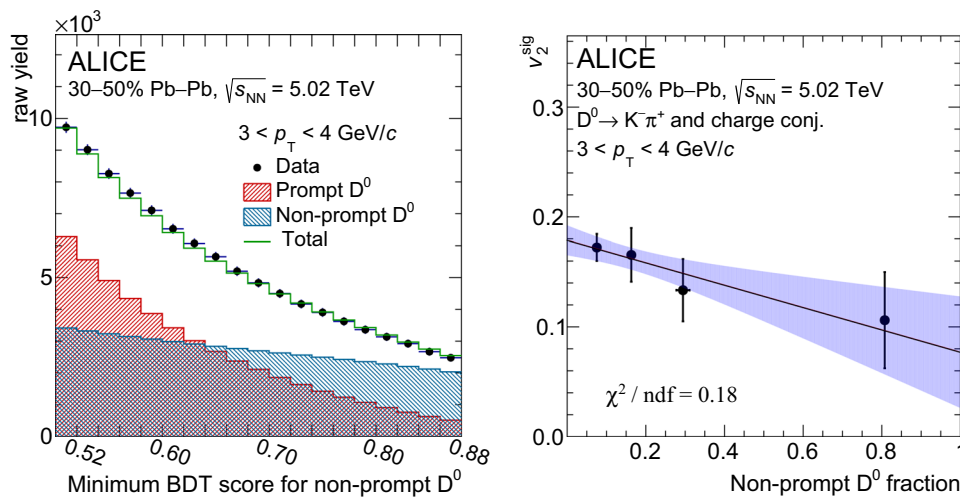


Fig. 2 Left panel: Example of the raw-yield distribution as a function of the minimum non-prompt D⁰-meson BDT score threshold to determine the non-prompt D⁰-meson fraction in $3 < p_T < 4 \text{ GeV}/c$. Right

panel: v_2^{sig} as a function of $f_{\text{non-prompt}}$ in $3 < p_T < 4 \text{ GeV}/c$. The blue band represents the 1 σ confidence interval obtained from the linear fit

Table 1 Summary of the systematic uncertainties on the measurement of the non-prompt D⁰-meson v_2 . The ranges of the uncertainties are quoted as absolute uncertainties, except those on the R_2 as relative uncertainty

p_T (GeV/c)	2–3	3–4	4–5	5–6	6–8	8–12
Signal extraction	0.011	0.012	0.011	0.011	0.012	0.013
Non-prompt fraction estimation	0.005	0.002	0.002	0.001	0.001	0.001
MC D-meson p_T distribution	0.004	0.004	0.002	0.001	0.001	0.001
R_2 determination (%)	0.5	0.5	0.5	0.5	0.5	0.5

ties. Table 1 summarises the estimated values of the systematic uncertainties for each p_T interval.

The systematic uncertainty of the signal extraction from the invariant-mass and v_2^{tot} distributions is due to a possible imperfect modelling of the signal and background distributions. It was evaluated by repeating the simultaneous fit with different configurations. In particular, the fit range, signal width within the statistical uncertainties obtained with prompt enhanced sample, and background fit functions used for the invariant-mass and v_2^{tot} distributions were varied. The systematic uncertainty was defined as the RMS of the distribution of the resulting $v_2^{\text{non-prompt}}$ obtained from all these variations. The second source of systematic uncertainty arises from the uncertainty on the determination of the $f_{\text{non-prompt}}$ of D⁰ mesons with the minimisation method described in Sect. 2. In this method, the raw yields and the efficiencies obtained with several sets of selections are used in order to extract the prompt and non-prompt components. It is therefore sensitive to possible imperfections of the data description in the MC simulations. They were therefore evaluated by using alternative sets of selections for the aforementioned χ^2 -minimisation approach [92]; the RMS of the resulting $v_2^{\text{non-prompt}}$ distribution was considered as the sys-

tematic uncertainty. The systematic effects due to possible differences between the real and simulated p_T spectra were estimated by applying different weights to the p_T distributions of prompt D⁰ mesons and of the parent beauty hadrons in the case of non-prompt D⁰ mesons. In the default analysis procedure, the weights were defined to match the shape given by FONLL in pp collisions [99,100] multiplied by the nuclear modification factor (R_{AA}) prediction from the TAMU model [55]. The FONLL spectrum multiplied by the R_{AA} from the LIDO model [101] was used as an alternative shape for the systematic evaluation. The effect due to flow-related modifications of the parent beauty-hadron p_T spectra was found to be negligible with respect to the assigned p_T -shape systematic uncertainty. The contribution of the SP denominator R_2 to the systematic uncertainty is due to the centrality dependence. It was evaluated as the difference of the centrality-integrated R_2 values with those obtained from weighted average R_2 values in narrow centrality intervals using the D⁰-meson yields as weights [52].

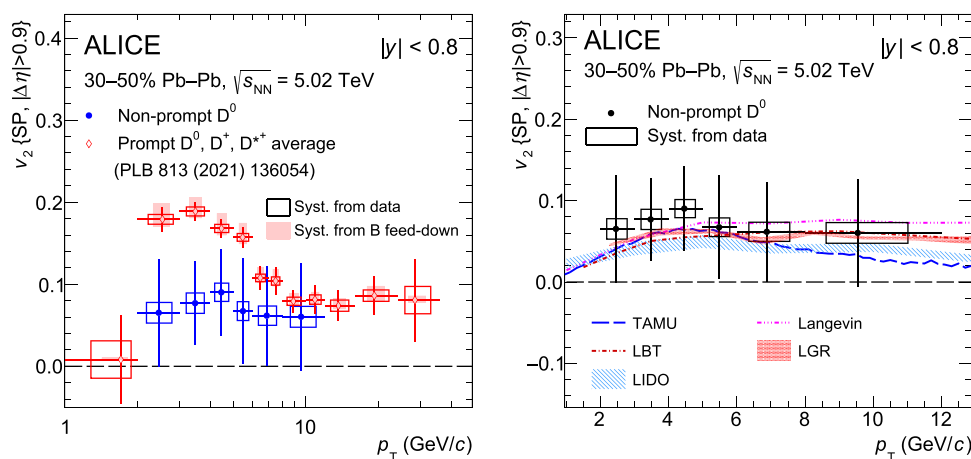


Fig. 3 Left panel: Elliptic flow v_2 of non-prompt D^0 mesons (blue points) and average of prompt non-strange D mesons [52] (red points) as a function of p_T in 30–50% Pb–Pb collisions at $\sqrt{s_{NN}} = 5.02$ TeV. The symbols are positioned at the average p_T of the reconstructed D^0

mesons. Statistical uncertainties are shown as vertical lines and systematic uncertainties as boxes. Right panel: Non-prompt D^0 -meson v_2 compared with model calculations [62, 101–107]

4 Results

The measured non-prompt D^0 -meson elliptic flow at midrapidity ($|y| < 0.8$) in the 30–50% centrality class is shown in Fig. 3 as a function of p_T . The weighted mean of the non-prompt D^0 -meson v_2 in the measured p_T range ($2 < p_T < 12$ GeV/c) is 2.7σ above 0. No significant p_T dependence of the v_2 is observed. The results obtained are compatible within uncertainties with those submitted for publication by CMS [73], which have smaller statistical uncertainty. In the left panel of Fig. 3, the non-prompt D^0 -meson v_2 is compared with the average v_2 of prompt $D^0, D^+,$ and D^{*+} mesons [52]. The non-prompt D^0 -meson v_2 is lower than that of prompt non-strange D mesons with 3.2σ significance in $2 < p_T < 8$ GeV/c, indicating a different degree of participation to the collective motion of the medium between charm and beauty quarks.

The measured v_2 of non-prompt D^0 mesons is compared with several theoretical models implementing beauty-quark transport in a hydrodynamically expanding QGP phase [62, 101–107] in the right panel of Fig. 3. All of the considered calculations include collisional interactions between beauty quarks and medium constituents. In addition, the LBT [62, 103], LIDO [101, 107], LGR [104], and Langevin [105, 106] models also include radiative processes. Beauty-quark hadronisation via coalescence is considered for all models in addition to the fragmentation mechanism. Although the models are implemented with different assumptions on the interactions in the QGP and hadronic phases, and on the medium expansion, all of them provide a reasonable description of the measurement within uncertainties. More precise measurements will further constrain model parameters, especially on the spatial diffusion coefficient of beauty

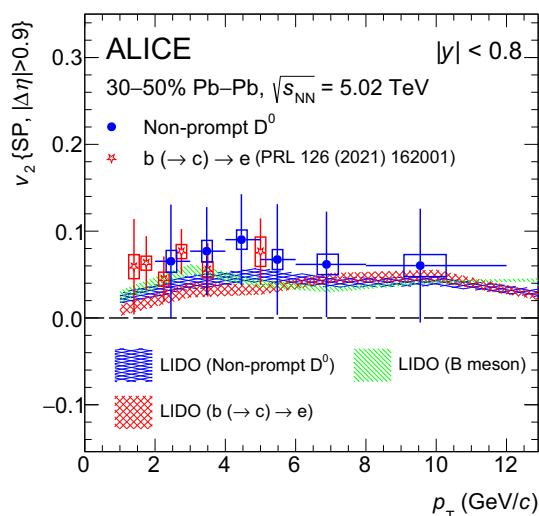


Fig. 4 Elliptic flow v_2 of non-prompt D^0 mesons (blue points) and electrons from beauty-hadron decays [71] (red points) as a function of p_T in 30–50% Pb–Pb collisions at $\sqrt{s_{NN}} = 5.02$ TeV, compared with the LIDO model predictions [101, 107]

quarks, which are implemented differently in the various models.

Figure 4 shows the comparison between the v_2 of electrons from beauty-hadron decays ($b(\rightarrow c) \rightarrow e$) [71] and the non-prompt D^0 -meson v_2 measurements. They are compatible in the common p_T interval within uncertainties. The LIDO model provides reasonable descriptions for these measurements and is consistent with the p_T shape in the data. Note that, the p_T of beauty-decay hadrons is not the same p_T of B mesons due to the decay kinematics. The good agreement between the predictions for B-meson and non-prompt D^0 -meson v_2 from LIDO indicates that the decay kinematics do

not play a significant role in the beauty-hadron v_2 measurements.

5 Conclusions

The measurement of the non-prompt D^0 -meson v_2 in midcentral Pb–Pb collisions (30–50% centrality class) at $\sqrt{s_{NN}} = 5.02$ TeV is presented in the transverse momentum interval $2 < p_T < 12$ GeV/ c . The non-prompt D^0 -meson v_2 is found to be positive with a significance of 2.7σ and it is lower by 3.2σ than the prompt non-strange D-meson v_2 (average of D^0 , D^+ , and D^{*+}) in the range $2 < p_T < 8$ GeV/ c . The measurement is important for the understanding of the degree of thermalisation of beauty quarks in the QGP. Future data samples to be collected with the upgraded ALICE detector in Run 3 will allow for higher-precision measurements of the non-prompt D^0 -meson v_2 and R_{AA} [108]. These measurements will provide important constraints to model predictions, and allow for accurate extraction of the spatial diffusion coefficient of beauty quarks.

Acknowledgements The ALICE Collaboration would like to thank all its engineers and technicians for their invaluable contributions to the construction of the experiment and the CERN accelerator teams for the outstanding performance of the LHC complex. The ALICE Collaboration gratefully acknowledges the resources and support provided by all Grid centres and the Worldwide LHC Computing Grid (WLCG) collaboration. The ALICE Collaboration acknowledges the following funding agencies for their support in building and running the ALICE detector: A. I. Alikhanyan National Science Laboratory (Yerevan Physics Institute) Foundation (ANSL), State Committee of Science and World Federation of Scientists (WFS), Armenia; Austrian Academy of Sciences, Austrian Science Fund (FWF) [M 2467-N36] and Nationalstiftung für Forschung, Technologie und Entwicklung, Austria; Ministry of Communications and High Technologies, National Nuclear Research Center, Azerbaijan; Conselho Nacional de Desenvolvimento Científico e Tecnológico (CNPq), Financiadora de Estudos e Projetos (Finep), Fundação de Amparo à Pesquisa do Estado de São Paulo (FAPESP) and Universidade Federal do Rio Grande do Sul (UFRGS), Brazil; Bulgarian Ministry of Education and Science, within the National Roadmap for Research Infrastructures 2020–2027 (object CERN), Bulgaria; Ministry of Education of China (MOEC), Ministry of Science and Technology of China (MSTC) and National Natural Science Foundation of China (NSFC), China; Ministry of Science and Education and Croatian Science Foundation, Croatia; Centro de Aplicaciones Tecnológicas y Desarrollo Nuclear (CEADEN), Cubaenergía, Cuba; Ministry of Education, Youth and Sports of the Czech Republic, Czech Republic; The Danish Council for Independent Research | Natural Sciences, the VILLUM FONDEN and Danish National Research Foundation (DNRF), Denmark; Helsinki Institute of Physics (HIP), Finland; Commissariat à l’Energie Atomique (CEA) and Institut National de Physique Nucléaire et de Physique des Particules (IN2P3) and Centre National de la Recherche Scientifique (CNRS), France; Bundesministerium für Bildung und Forschung (BMBF) and GSI Helmholtzzentrum für Schwerionenforschung GmbH, Germany; General Secretariat for Research and Technology, Ministry of Education, Research and Religions, Greece; National Research, Development and Innovation Office, Hungary; Department of Atomic Energy Government of India (DAE), Department of Science and Technology, Government of India (DST), University Grants Commission, Government of

India (UGC) and Council of Scientific and Industrial Research (CSIR), India; National Research and Innovation Agency-BRIN, Indonesia; Istituto Nazionale di Fisica Nucleare (INFN), Italy; Japanese Ministry of Education, Culture, Sports, Science and Technology (MEXT) and Japan Society for the Promotion of Science (JSPS) KAKENHI, Japan; Consejo Nacional de Ciencia (CONACYT) y Tecnología, through Fondo de Cooperación Internacional en Ciencia y Tecnología (FONCICYT) and Dirección General de Asuntos del Personal Académico (DGAPA), Mexico; Nederlandse Organisatie voor Wetenschappelijk Onderzoek (NWO), Netherlands; The Research Council of Norway, Norway; Commission on Science and Technology for Sustainable Development in the South (COMSATS), Pakistan; Pontificia Universidad Católica del Perú, Peru; Ministry of Education and Science, National Science Centre and WUT ID-UB, Poland; Korea Institute of Science and Technology Information and National Research Foundation of Korea (NRF), Republic of Korea; Ministry of Education and Scientific Research, Institute of Atomic Physics, Ministry of Research and Innovation and Institute of Atomic Physics and University Politehnica of Bucharest, Romania; Ministry of Education, Science, Research and Sport of the Slovak Republic, Slovakia; National Research Foundation of South Africa, South Africa; Swedish Research Council (VR) and Knut and Alice Wallenberg Foundation (KAW), Sweden; European Organization for Nuclear Research, Switzerland; Suranaree University of Technology (SUT), National Science and Technology Development Agency (NSTDA), Thailand Science Research and Innovation (TSRI) and National Science, Research and Innovation Fund (NSRF), Thailand; Turkish Energy, Nuclear and Mineral Research Agency (TENMAK), Turkey; National Academy of Sciences of Ukraine, Ukraine; Science and Technology Facilities Council (STFC), United Kingdom; National Science Foundation of the United States of America (NSF) and United States Department of Energy, Office of Nuclear Physics (DOE NP), United States of America. In addition, individual groups or members have received support from: European Research Council, Strong 2020-Horizon 2020 (Grant nos. 950692, 824093), European Union; Academy of Finland (Center of Excellence in Quark Matter) (Grant nos. 346327, 346328), Finland.

Data Availability Statement This manuscript has associated data in a data repository. [Authors’ comment: Manuscript has associated data in a HEPData repository at <https://www.hepdata.net/record/145800>.]

Open Access This article is licensed under a Creative Commons Attribution 4.0 International License, which permits use, sharing, adaptation, distribution and reproduction in any medium or format, as long as you give appropriate credit to the original author(s) and the source, provide a link to the Creative Commons licence, and indicate if changes were made. The images or other third party material in this article are included in the article’s Creative Commons licence, unless indicated otherwise in a credit line to the material. If material is not included in the article’s Creative Commons licence and your intended use is not permitted by statutory regulation or exceeds the permitted use, you will need to obtain permission directly from the copyright holder. To view a copy of this licence, visit <http://creativecommons.org/licenses/by/4.0/>.

Funded by SCOAP³. SCOAP³ supports the goals of the International Year of Basic Sciences for Sustainable Development.

References

1. NA50 Collaboration, M.C. Abreu et al., Evidence for deconfinement of quarks and gluons from the J/ψ suppression pattern measured in Pb–Pb collisions at the CERN-SPS. Phys. Lett. B **477**, 28–36 (2000). [https://doi.org/10.1016/S0370-2693\(00\)00237-9](https://doi.org/10.1016/S0370-2693(00)00237-9)

2. WA97 Collaboration, E. Andersen et al., Strangeness enhancement at mid-rapidity in Pb–Pb collisions at 158 A GeV/c. *Phys. Lett. B* **449**, 401–406 (1999). [https://doi.org/10.1016/S0370-2693\(99\)00140-9](https://doi.org/10.1016/S0370-2693(99)00140-9)
3. BRAHMS Collaboration, I. Arsene et al., Quark gluon plasma and color glass condensate at RHIC? The perspective from the BRAHMS experiment. *Nucl. Phys. A* **757**, 1–27 (2005). <https://doi.org/10.1016/j.nuclphysa.2005.02.130>. [arXiv:nucl-ex/0410020](https://arxiv.org/abs/nucl-ex/0410020)
4. PHENIX Collaboration, K. Adcox et al., Formation of dense partonic matter in relativistic nucleus–nucleus collisions at RHIC: experimental evaluation by the PHENIX collaboration. *Nucl. Phys. A* **757**, 184–283 (2005). <https://doi.org/10.1016/j.nuclphysa.2005.03.086>. [arXiv:nucl-ex/0410003](https://arxiv.org/abs/nucl-ex/0410003)
5. PHOBOS Collaboration, B.B. Back et al., The PHOBOS perspective on discoveries at RHIC. *Nucl. Phys. A* **757**, 28–101 (2005). <https://doi.org/10.1016/j.nuclphysa.2005.03.084>. [arXiv:nucl-ex/0410022](https://arxiv.org/abs/nucl-ex/0410022)
6. STAR Collaboration, J. Adams et al., Experimental and theoretical challenges in the search for the quark–gluon plasma: the STAR Collaboration’s critical assessment of the evidence from RHIC collisions. *Nucl. Phys. A* **757**, 102–183 (2005). <https://doi.org/10.1016/j.nuclphysa.2005.03.085>. [arXiv:nucl-ex/0501009](https://arxiv.org/abs/nucl-ex/0501009)
7. G. Roland, K. Safarik, P. Steinberg, Heavy-ion collisions at the LHC. *Prog. Part. Nucl. Phys.* **77**, 70–127 (2014). <https://doi.org/10.1016/j.pnpnp.2014.05.001>
8. P. Braun-Munzinger, V. Koch, T. Schäfer, J. Stachel, Properties of hot and dense matter from relativistic heavy ion collisions. *Phys. Rep.* **621**, 76–126 (2016). <https://doi.org/10.1016/j.physrep.2015.12.003>. [arXiv:1510.00442](https://arxiv.org/abs/1510.00442) [nucl-th]
9. ALICE Collaboration, The ALICE experiment—a journey through QCD. [arXiv:2211.04384](https://arxiv.org/abs/2211.04384) [nucl-ex] (review)
10. U. Heinz, R. Snellings, Collective flow and viscosity in relativistic heavy-ion collisions. *Annu. Rev. Nucl. Part. Sci.* **63**, 123–151 (2013). <https://doi.org/10.1146/annurev-nucl-102212-170540>. [arXiv:1301.2826](https://arxiv.org/abs/1301.2826) [nucl-th]
11. F.-M. Liu, S.-X. Liu, Quark-gluon plasma formation time and direct photons from heavy ion collisions. *Phys. Rev. C* **89**, 034906 (2014). <https://doi.org/10.1103/PhysRevC.89.034906>. [arXiv:1212.6587](https://arxiv.org/abs/1212.6587) [nucl-th]
12. A. Andronic et al., Heavy-flavour and quarkonium production in the LHC era: from proton–proton to heavy-ion collisions. *Eur. Phys. J. C* **76**, 107 (2016). <https://doi.org/10.1140/epjc/s10052-015-3819-5>. [arXiv:1506.03981](https://arxiv.org/abs/1506.03981) [nucl-ex]
13. E. Braaten, M.H. Thoma, Energy loss of a heavy quark in the quark-gluon plasma. *Phys. Rev. D* **44**, R2625 (1991). <https://doi.org/10.1103/PhysRevD.44.R2625>
14. PHENIX Collaboration, A. Adare et al., Heavy quark production in $p + p$ and energy loss and flow of heavy quarks in Au+Au collisions at $\sqrt{s_{NN}} = 200$ GeV. *Phys. Rev. C* **84**, 044905 (2011). <https://doi.org/10.1103/PhysRevC.84.044905>. [arXiv:1005.1627](https://arxiv.org/abs/1005.1627) [nucl-ex]
15. STAR Collaboration, B. Abelev et al., Transverse momentum and centrality dependence of high- p_T non-photonic electron suppression in Au+Au collisions at $\sqrt{s_{NN}} = 200$ GeV. *Phys. Rev. Lett.* **98**, 192301 (2007). <https://doi.org/10.1103/PhysRevLett.98.192301>. [arXiv:nucl-ex/0607012](https://arxiv.org/abs/nucl-ex/0607012). [Erratum: *Phys. Rev. Lett.* **106**, 159902 (2011)]
16. STAR Collaboration, L. Adamczyk et al., Observation of D^0 meson nuclear modifications in Au+Au collisions at $\sqrt{s_{NN}} = 200$ GeV. *Phys. Rev. Lett.* **113**, 142301 (2014). <https://doi.org/10.1103/PhysRevLett.113.142301>. [arXiv:1404.6185](https://arxiv.org/abs/1404.6185) [nucl-ex]. [Erratum: *Phys. Rev. Lett.* **121**, 229901 (2018)]
17. PHENIX Collaboration, S.S. Adler et al., Nuclear modification of electron spectra and implications for heavy quark energy loss in Au+Au collisions at $\sqrt{s_{NN}} = 200$ GeV. *Phys. Rev. Lett.* **96**, 032301 (2006). <https://doi.org/10.1103/PhysRevLett.96.032301>. [arXiv:nucl-ex/0510047](https://arxiv.org/abs/nucl-ex/0510047)
18. PHENIX Collaboration, A. Adare et al., Single electron yields from semileptonic charm and bottom hadron decays in Au+Au collisions at $\sqrt{s_{NN}} = 200$ GeV. *Phys. Rev. C* **93**, 034904 (2016). <https://doi.org/10.1103/PhysRevC.93.034904>. [arXiv:1509.04662](https://arxiv.org/abs/1509.04662) [nucl-ex]
19. ALICE Collaboration, J. Adam et al., Transverse momentum dependence of D-meson production in Pb–Pb collisions at $\sqrt{s_{NN}} = 2.76$ TeV. *JHEP* **03**, 081 (2016). [https://doi.org/10.1007/JHEP03\(2016\)081](https://doi.org/10.1007/JHEP03(2016)081). [arXiv:1509.06888](https://arxiv.org/abs/1509.06888) [nucl-ex]
20. ALICE Collaboration, B. Abelev et al., Production of muons from heavy flavour decays at forward rapidity in pp and Pb–Pb collisions at $\sqrt{s_{NN}} = 2.76$ TeV. *Phys. Rev. Lett.* **109**, 112301 (2012). <https://doi.org/10.1103/PhysRevLett.109.112301>. [arXiv:1205.6443](https://arxiv.org/abs/1205.6443) [hep-ex]
21. ALICE Collaboration, J. Adam et al., Measurement of the production of high- p_T electrons from heavy-flavour hadron decays in Pb–Pb collisions at $\sqrt{s_{NN}} = 2.76$ TeV. *Phys. Lett. B* **771**, 467–481 (2017). <https://doi.org/10.1016/j.physletb.2017.05.060>. [arXiv:1609.07104](https://arxiv.org/abs/1609.07104) [nucl-ex]
22. ALICE Collaboration, J. Adam et al., Measurement of electrons from beauty-hadron decays in p–Pb collisions at $\sqrt{s_{NN}} = 5.02$ TeV and Pb–Pb collisions at $\sqrt{s_{NN}} = 2.76$ TeV. *JHEP* **07**, 052 (2017). [https://doi.org/10.1007/JHEP07\(2017\)052](https://doi.org/10.1007/JHEP07(2017)052). [arXiv:1609.03898](https://arxiv.org/abs/1609.03898) [nucl-ex]
23. CMS Collaboration, V. Khachatryan et al., Suppression and azimuthal anisotropy of prompt and nonprompt J/ψ production in PbPb collisions at $\sqrt{s_{NN}} = 2.76$ TeV. *Eur. Phys. J. C* **77**, 252 (2017). <https://doi.org/10.1140/epjc/s10052-017-4781-1>. [arXiv:1610.00613](https://arxiv.org/abs/1610.00613) [nucl-ex]
24. CMS Collaboration, A.M. Sirunyan et al., Nuclear modification factor of D^0 mesons in PbPb collisions at $\sqrt{s_{NN}} = 5.02$ TeV. *Phys. Lett. B* **782**, 474–496 (2018). <https://doi.org/10.1016/j.physletb.2018.05.074>. [arXiv:1708.04962](https://arxiv.org/abs/1708.04962) [nucl-ex]
25. ALICE Collaboration, S. Acharya et al., Measurement of D^0 , D^+ , D^{*+} and D_s^+ production in Pb–Pb collisions at $\sqrt{s_{NN}} = 5.02$ TeV. *JHEP* **10**, 174 (2018). [https://doi.org/10.1007/JHEP10\(2018\)174](https://doi.org/10.1007/JHEP10(2018)174). [arXiv:1804.09083](https://arxiv.org/abs/1804.09083) [nucl-ex]
26. CMS Collaboration, A.M. Sirunyan et al., Measurement of B_s^0 meson production in pp and PbPb collisions at $\sqrt{s_{NN}} = 5.02$ TeV. *Phys. Lett. B* **796**, 168–190 (2019). <https://doi.org/10.1016/j.physletb.2019.07.014>. [arXiv:1810.03022](https://arxiv.org/abs/1810.03022) [hep-ex]
27. CMS Collaboration, A.M. Sirunyan et al., Measurement of the B^{\pm} meson nuclear modification factor in Pb–Pb collisions at $\sqrt{s_{NN}} = 5.02$ TeV. *Phys. Rev. Lett.* **119**, 152301 (2017). <https://doi.org/10.1103/PhysRevLett.119.152301>. [arXiv:1705.04727](https://arxiv.org/abs/1705.04727) [hep-ex]
28. ALICE Collaboration, S. Acharya et al., Prompt D^0 , D^+ , and D^{*+} production in Pb–Pb collisions at $\sqrt{s_{NN}} = 5.02$ TeV. *JHEP* **01**, 174 (2022). [https://doi.org/10.1007/JHEP01\(2022\)174](https://doi.org/10.1007/JHEP01(2022)174). [arXiv:2110.09420](https://arxiv.org/abs/2110.09420) [nucl-ex]
29. ALICE Collaboration, S. Acharya et al., Measurement of prompt D_s^+ -meson production and azimuthal anisotropy in Pb–Pb collisions at $\sqrt{s_{NN}} = 5.02$ TeV. *Phys. Lett. B* **827**, 136986 (2022). <https://doi.org/10.1016/j.physletb.2022.136986>. [arXiv:2110.10006](https://arxiv.org/abs/2110.10006) [nucl-ex]
30. ALICE Collaboration, S. Acharya et al., Constraining hadronization mechanisms with Λ_c^+/D^0 production ratios in Pb–Pb collisions at $\sqrt{s_{NN}} = 5.02$ TeV. *Phys. Lett. B* **839**, 137796 (2023). <https://doi.org/10.1016/j.physletb.2023.137796>. [arXiv:2112.08156](https://arxiv.org/abs/2112.08156) [nucl-ex]
31. ALICE Collaboration, S. Acharya et al., Measurement of beauty production via non-prompt D^0 mesons in Pb–Pb collisions at $\sqrt{s_{NN}} = 5.02$ TeV. *JHEP* **12**, 126 (2022). [https://doi.org/10.1007/JHEP12\(2022\)126](https://doi.org/10.1007/JHEP12(2022)126). [arXiv:2202.00815](https://arxiv.org/abs/2202.00815) [nucl-ex]

32. ALICE Collaboration, S. Acharya et al., Measurement of beauty-strange meson production in Pb–Pb collisions at $\sqrt{s_{NN}} = 5.02$ TeV via non-prompt D_s^+ mesons. *Phys. Lett. B* **846**, 137561 (2023). <https://doi.org/10.1016/j.physletb.2022.137561>. [arXiv:2204.10386](https://arxiv.org/abs/2204.10386) [nucl-ex]
33. ALICE Collaboration, S. Acharya et al., Measurement of electrons from beauty-hadron decays in pp and Pb–Pb collisions at $\sqrt{s_{NN}} = 5.02$ TeV. *Phys. Rev. C* **108**, 034906 (2023). <https://doi.org/10.1103/PhysRevC.108.034906>. [arXiv:2211.13985](https://arxiv.org/abs/2211.13985) [nucl-ex]
34. J.-Y. Ollitrault, Anisotropy as a signature of transverse collective flow. *Phys. Rev. D* **46**, 229–245 (1992). <https://doi.org/10.1103/PhysRevD.46.229>
35. S. Voloshin, Y. Zhang, Flow study in relativistic nuclear collisions by Fourier expansion of Azimuthal particle distributions. *Z. Phys. C* **70**, 665–672 (1996). <https://doi.org/10.1007/s002880050141>. [arXiv:hep-ph/9407282](https://arxiv.org/abs/hep-ph/9407282)
36. S. Batsouli, S. Kelly, M. Gyulassy, J.L. Nagle, Does the charm flow at RHIC? *Phys. Lett. B* **557**, 26–32 (2003). [https://doi.org/10.1016/S0370-2693\(03\)00175-8](https://doi.org/10.1016/S0370-2693(03)00175-8). [arXiv:nucl-th/0212068](https://arxiv.org/abs/nucl-th/0212068)
37. D. Molnar, Charm elliptic flow from quark coalescence dynamics. *J. Phys. G* **31**, S421–S428 (2005). <https://doi.org/10.1088/0954-3899/31/4/052>. [arXiv:nucl-th/0410041](https://arxiv.org/abs/nucl-th/0410041)
38. V. Greco, C.M. Ko, R. Rapp, Quark coalescence for charmed mesons in ultrarelativistic heavy ion collisions. *Phys. Lett. B* **595**, 202–208 (2004). <https://doi.org/10.1016/j.physletb.2004.06.064>. [arXiv:nucl-th/0312100](https://arxiv.org/abs/nucl-th/0312100)
39. M. Gyulassy, I. Vitev, X.N. Wang, High p_T azimuthal asymmetry in noncentral A+A at RHIC. *Phys. Rev. Lett.* **86**, 2537–2540 (2001). <https://doi.org/10.1103/PhysRevLett.86.2537>. [arXiv:nucl-th/0012092](https://arxiv.org/abs/nucl-th/0012092)
40. E.V. Shuryak, The Azimuthal asymmetry at large PT seem to be too large for a ‘jet quenching’. *Phys. Rev. C* **66**, 027902 (2002). <https://doi.org/10.1103/PhysRevC.66.027902>. [arXiv:nucl-th/0112042](https://arxiv.org/abs/nucl-th/0112042)
41. PHENIX Collaboration, A. Adare et al., Energy loss and flow of heavy quarks in Au+Au collisions at $\sqrt{s_{NN}} = 200$ GeV. *Phys. Rev. Lett.* **98**, 172301 (2007). <https://doi.org/10.1103/PhysRevLett.98.172301>. [arXiv:nucl-ex/0611018](https://arxiv.org/abs/nucl-ex/0611018)
42. STAR Collaboration, L. Adamczyk et al., Elliptic flow of electrons from heavy-flavor hadron decays in Au+Au collisions at $\sqrt{s_{NN}} = 200, 62.4,$ and 39 GeV. *Phys. Rev. C* **95**, 034907 (2017). <https://doi.org/10.1103/PhysRevC.95.034907>. [arXiv:1405.6348](https://arxiv.org/abs/1405.6348) [hep-ex]
43. STAR Collaboration, L. Adamczyk et al., Measurement of D^0 azimuthal anisotropy at midrapidity in Au+Au collisions at $\sqrt{s_{NN}} = 200$ GeV. *Phys. Rev. Lett.* **118**, 212301 (2017). <https://doi.org/10.1103/PhysRevLett.118.212301>. [arXiv:1701.06060](https://arxiv.org/abs/1701.06060) [nucl-ex]
44. ALICE Collaboration, B. Abelev et al., D meson elliptic flow in non-central Pb–Pb collisions at $\sqrt{s_{NN}} = 2.76$ TeV. *Phys. Rev. Lett.* **111**, 102301 (2013). <https://doi.org/10.1103/PhysRevLett.111.102301>. [arXiv:1305.2707](https://arxiv.org/abs/1305.2707) [nucl-ex]
45. ALICE Collaboration, B. Abelev et al., Azimuthal anisotropy of D meson production in Pb–Pb collisions at $\sqrt{s_{NN}} = 2.76$ TeV. *Phys. Rev. C* **90**, 034904 (2014). <https://doi.org/10.1103/PhysRevC.90.034904>. [arXiv:1405.2001](https://arxiv.org/abs/1405.2001) [nucl-ex]
46. ALICE Collaboration, J. Adam et al., Elliptic flow of electrons from heavy-flavour hadron decays at mid-rapidity in Pb–Pb collisions at $\sqrt{s_{NN}} = 2.76$ TeV. *JHEP* **09**, 028 (2016). [https://doi.org/10.1007/JHEP09\(2016\)028](https://doi.org/10.1007/JHEP09(2016)028). [arXiv:1606.00321](https://arxiv.org/abs/1606.00321) [nucl-ex]
47. ALICE Collaboration, J. Adam et al., Elliptic flow of muons from heavy-flavour hadron decays at forward rapidity in Pb–Pb collisions at $\sqrt{s_{NN}} = 2.76$ TeV. *Phys. Lett. B* **753**, 41–56 (2016). <https://doi.org/10.1016/j.physletb.2015.11.059>. [arXiv:1507.03134](https://arxiv.org/abs/1507.03134) [nucl-ex]
48. ALICE Collaboration, S. Acharya et al., D-meson azimuthal anisotropy in midcentral Pb–Pb collisions at $\sqrt{s_{NN}} = 5.02$ TeV. *Phys. Rev. Lett.* **120**, 102301 (2018). <https://doi.org/10.1103/PhysRevLett.120.102301>. [arXiv:1707.01005](https://arxiv.org/abs/1707.01005) [nucl-ex]
49. CMS Collaboration, A.M. Sirunyan et al., Measurement of prompt D^0 meson azimuthal anisotropy in Pb–Pb collisions at $\sqrt{s_{NN}} = 5.02$ TeV. *Phys. Rev. Lett.* **120**, 202301 (2018). <https://doi.org/10.1103/PhysRevLett.120.202301>. [arXiv:1708.03497](https://arxiv.org/abs/1708.03497) [nucl-ex]
50. ALICE Collaboration, S. Acharya et al., Event-shape engineering for the D-meson elliptic flow in mid-central Pb–Pb collisions at $\sqrt{s_{NN}} = 5.02$ TeV. *JHEP* **02**, 150 (2019). [https://doi.org/10.1007/JHEP02\(2019\)150](https://doi.org/10.1007/JHEP02(2019)150). [arXiv:1809.09371](https://arxiv.org/abs/1809.09371) [nucl-ex]
51. CMS Collaboration, A.M. Sirunyan et al., Measurement of prompt D^0 meson azimuthal anisotropy in Pb–Pb collisions at $\sqrt{s_{NN}} = 5.02$ TeV. *Phys. Rev. Lett.* **120**, 202301 (2018). <https://doi.org/10.1103/PhysRevLett.120.202301>. [arXiv:1708.03497](https://arxiv.org/abs/1708.03497) [nucl-ex]
52. ALICE Collaboration, S. Acharya et al., Transverse-momentum and event-shape dependence of D-meson flow harmonics in Pb–Pb collisions at $\sqrt{s_{NN}} = 5.02$ TeV. *Phys. Lett. B* **813**, 136054 (2021). <https://doi.org/10.1016/j.physletb.2020.136054>. [arXiv:2005.11131](https://arxiv.org/abs/2005.11131) [nucl-ex]
53. CMS Collaboration, A.M. Sirunyan et al., Measurement of prompt D^0 and \bar{D}^0 meson azimuthal anisotropy and search for strong electric fields in PbPb collisions at $\sqrt{s_{NN}} = 5.02$ TeV. *Phys. Lett. B* **816**, 136253 (2021). <https://doi.org/10.1016/j.physletb.2021.136253>. [arXiv:2009.12628](https://arxiv.org/abs/2009.12628) [hep-ex]
54. J. Uphoff, O. Fochler, Z. Xu, C. Greiner, Open heavy flavor in Pb+Pb collisions at $\sqrt{s} = 2.76$ TeV within a transport model. *Phys. Lett. B* **717**, 430–435 (2012). <https://doi.org/10.1016/j.physletb.2012.09.069>. [arXiv:1205.4945](https://arxiv.org/abs/1205.4945) [hep-ph]
55. M. He, R.J. Fries, R. Rapp, Heavy flavor at the large hadron collider in a strong coupling approach. *Phys. Lett. B* **735**, 445–450 (2014). <https://doi.org/10.1016/j.physletb.2014.05.050>. [arXiv:1401.3817](https://arxiv.org/abs/1401.3817) [nucl-th]
56. M. Monteno, W.M. Alberico, A. Beraudo, A. De Pace, A. Molinari, M. Nardi, F. Prino, Heavy-flavor dynamics in nucleus-nucleus collisions: from RHIC to LHC. *J. Phys. G* **38**, 124144 (2011). <https://doi.org/10.1088/0954-3899/38/12/124144>. [arXiv:1107.0256](https://arxiv.org/abs/1107.0256) [hep-ph]
57. S. Cao, G.-Y. Qin, S.A. Bass, Heavy-quark dynamics and hadronization in ultrarelativistic heavy-ion collisions: collisional versus radiative energy loss. *Phys. Rev. C* **88**, 044907 (2013). <https://doi.org/10.1103/PhysRevC.88.044907>. [arXiv:1308.0617](https://arxiv.org/abs/1308.0617) [nucl-th]
58. T. Song, H. Berrehrah, D. Cabrera, W. Cassing, E. Bratkovskaya, Charm production in Pb + Pb collisions at energies available at the CERN Large Hadron Collider. *Phys. Rev. C* **93**, 034906 (2016). <https://doi.org/10.1103/PhysRevC.93.034906>. [arXiv:1512.00891](https://arxiv.org/abs/1512.00891) [nucl-th]
59. M. Nahrgang, J. Aichelin, P.B. Gossiaux, K. Werner, Influence of hadronic bound states above T_c on heavy-quark observables in Pb + Pb collisions at the CERN Large Hadron Collider. *Phys. Rev. C* **89**, 014905 (2014). <https://doi.org/10.1103/PhysRevC.89.014905>. [arXiv:1305.6544](https://arxiv.org/abs/1305.6544) [hep-ph]
60. J. Uphoff, O. Fochler, Z. Xu, C. Greiner, Elastic and radiative heavy quark interactions in ultra-relativistic heavy-ion collisions. *J. Phys. G* **42**, 115106 (2015). <https://doi.org/10.1088/0954-3899/42/11/115106>. [arXiv:1408.2964](https://arxiv.org/abs/1408.2964) [hep-ph]
61. A. Beraudo, A. De Pace, M. Monteno, M. Nardi, F. Prino, Heavy flavors in heavy-ion collisions: quenching, flow and correlations. *Eur. Phys. J. C* **75**, 121 (2015). <https://doi.org/10.1140/epjc/s10052-015-3336-6>. [arXiv:1410.6082](https://arxiv.org/abs/1410.6082) [hep-ph]
62. S. Cao, T. Luo, G.-Y. Qin, X.-N. Wang, Heavy and light flavor jet quenching at RHIC and LHC energies. *Phys. Lett. B* **777**,















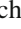

















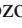





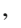






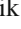
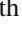




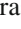


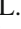

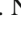
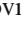





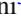










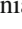

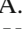


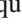

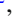
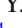




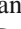


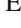
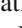





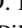
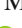
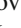





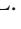





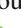









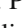
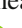
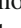


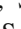
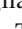


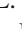














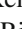




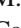





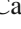
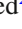

















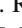







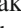


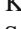





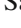






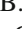


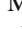



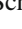
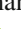
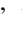








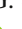
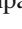

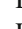








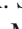
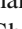





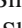
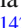




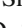
















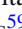


























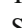



- 255–259 (2018). <https://doi.org/10.1016/j.physletb.2017.12.023>. arXiv:1703.00822 [nucl-th]
63. A. Beraudo, A. De Pace, M. Monteno, M. Nardi, F. Prino, Rapidity dependence of heavy-flavour production in heavy-ion collisions within a full 3+1 transport approach: quenching, elliptic and directed flow. *JHEP* **05**, 279 (2021). [https://doi.org/10.1007/JHEP05\(2021\)279](https://doi.org/10.1007/JHEP05(2021)279). arXiv:2102.08064 [hep-ph]
 64. G.D. Moore, D. Teaney, How much do heavy quarks thermalize in a heavy ion collision? *Phys. Rev. C* **71**, 064904 (2005). <https://doi.org/10.1103/PhysRevC.71.064904>. arXiv:hep-ph/0412346
 65. A. Francis, O. Kaczmarek, M. Laine, T. Neuhaus, H. Ohno, Non-perturbative estimate of the heavy quark momentum diffusion coefficient. *Phys. Rev. D* **92**, 116003 (2015). <https://doi.org/10.1103/PhysRevD.92.116003>. arXiv:1508.04543 [hep-lat]
 66. S.Y.F. Liu, R. Rapp, Spectral and transport properties of quark-gluon plasma in a nonperturbative approach. *Eur. Phys. J. A* **56**, 44 (2020). <https://doi.org/10.1140/epja/s10050-020-00024-z>. arXiv:1612.09138 [nucl-th]
 67. F. Riek, R. Rapp, Quarkonia and heavy-quark relaxation times in the quark-gluon plasma. *Phys. Rev. C* **82**, 035201 (2010). <https://doi.org/10.1103/PhysRevC.82.035201>. arXiv:1005.0769 [hep-ph]
 68. F. Capellino, A. Beraudo, A. Dubla, S. Floerchinger, S. Masciocchi, J. Pawlowski, I. Selyuzhenkov, Fluid-dynamic approach to heavy-quark diffusion in the quark-gluon plasma. *Phys. Rev. D* **106**, 034021 (2022). <https://doi.org/10.1103/PhysRevD.106.034021>. arXiv:2205.07692 [nucl-th]
 69. CMS Collaboration, V. Khachatryan et al., Suppression and azimuthal anisotropy of prompt and nonprompt J/ψ production in PbPb collisions at $\sqrt{s_{NN}} = 2.76$ TeV. *Eur. Phys. J. C* **77**, 252 (2017). <https://doi.org/10.1140/epjc/s10052-017-4781-1>. arXiv:1610.00613 [nucl-ex]
 70. ATLAS Collaboration, M. Aaboud et al., Prompt and non-prompt J/ψ elliptic flow in Pb+Pb collisions at $\sqrt{s_{NN}} = 5.02$ TeV with the ATLAS detector. *Eur. Phys. J. C* **78**, 784 (2018). <https://doi.org/10.1140/epjc/s10052-018-6243-9>. arXiv:1807.05198 [nucl-ex]
 71. ALICE Collaboration, S. Acharya et al., Elliptic flow of electrons from beauty-hadron decays in Pb–Pb collisions at $\sqrt{s_{NN}} = 5.02$ TeV. *Phys. Rev. Lett.* **126**, 162001 (2021). <https://doi.org/10.1103/PhysRevLett.126.162001>. arXiv:2005.11130 [nucl-ex]
 72. ATLAS Collaboration, G. Aad et al., Measurement of azimuthal anisotropy of muons from charm and bottom hadrons in Pb+Pb collisions at $\sqrt{s_{NN}} = 5.02$ TeV with the ATLAS detector. *Phys. Lett. B* **807**, 135595 (2020). <https://doi.org/10.1016/j.physletb.2020.135595>. arXiv:2003.03565 [nucl-ex]
 73. CMS Collaboration, Measurements of azimuthal anisotropy of nonprompt D^0 mesons in PbPb collisions at $\sqrt{s_{NN}} = 5.02$ TeV. arXiv:2212.01636 [nucl-ex] (review)
 74. M. Luzum, J.-Y. Ollitrault, Eliminating experimental bias in anisotropic-flow measurements of high-energy nuclear collisions. *Phys. Rev. C* **87**, 044907 (2013). <https://doi.org/10.1103/PhysRevC.87.044907>. arXiv:1209.2323 [nucl-ex]
 75. S.A. Voloshin, A.M. Poskanzer, R. Snellings, Collective phenomena in non-central nuclear collisions. *Landolt-Bornstein* **23**, 293–333 (2010). https://doi.org/10.1007/978-3-642-01539-7_10. arXiv:0809.2949 [nucl-ex]
 76. ALICE Collaboration, B. Abelev et al., Performance of the ALICE experiment at the CERN LHC. *Int. J. Mod. Phys. A* **29**, 1430044 (2014). <https://doi.org/10.1142/S0217751X14300440>. arXiv:1402.4476 [nucl-ex]
 77. ALICE Collaboration, K. Aamodt et al., The ALICE experiment at the CERN LHC. *JINST* **3**, S08002 (2008). <https://doi.org/10.1088/1748-0221/3/08/S08002>
 78. ALICE Collaboration, K. Aamodt et al., Alignment of the ALICE inner tracking system with cosmic-ray tracks. *JINST* **5**, P03003 (2010). <https://doi.org/10.1088/1748-0221/5/03/P03003>. arXiv:1001.0502 [physics.ins-det]
 79. J. Alme et al., The ALICE TPC, a large 3-dimensional tracking device with fast readout for ultra-high multiplicity events. *Nucl. Instrum. Methods A* **622**, 316–367 (2010). <https://doi.org/10.1016/j.nima.2010.04.042>. arXiv:1001.1950 [physics.ins-det]
 80. A. Akindinov et al., Performance of the ALICE Time-Of-Flight detector at the LHC. *Eur. Phys. J. Plus* **128**, 44 (2013). <https://doi.org/10.1140/epjp/i2013-13044-x>
 81. ALICE Collaboration, E. Abbas et al., Performance of the ALICE VZERO system. *JINST* **8**, P10016 (2013). <https://doi.org/10.1088/1748-0221/8/10/P10016>. arXiv:1306.3130 [nucl-ex]
 82. R. Arnaldi et al., The zero degree calorimeters for the ALICE experiment. *Nucl. Instrum. Methods A* **581**, 397–401 (2007). <https://doi.org/10.1016/j.nima.2008.04.009> [Erratum: *Nucl. Instrum. Methods A* **604**, 765 (2009)]
 83. ALICE Collaboration, J. Adam et al., Centrality dependence of the charged-particle multiplicity density at midrapidity in Pb–Pb collisions at $\sqrt{s_{NN}} = 5.02$ TeV. *Phys. Rev. Lett.* **116**, 222302 (2016). <https://doi.org/10.1103/PhysRevLett.116.222302>. arXiv:1512.06104 [nucl-ex]
 84. ALICE Collaboration, Centrality determination in heavy ion collisions. Technical Report. ALICE-PUBLIC-2018-011 (2018). <http://cds.cern.ch/record/2636623>
 85. Particle Data Group Collaboration, R.L. Workman et al., Review of particle physics. *PTEP* **2022**, 083C01 (2022). <https://doi.org/10.1093/ptep/ptac097>
 86. T. Chen, C. Guestrin, XGBoost: a scalable tree boosting system, in *Proceedings of the 22nd ACM SIGKDD International Conference on Knowledge Discovery and Data Mining* (2016), pp. 785–794. <https://doi.org/10.1145/2939672.2939785>. arXiv:1603.02754 [cs.LG]
 87. X.-N. Wang, M. Gyulassy, HIJING: a Monte Carlo model for multiple jet production in pp, pA and AA collisions. *Phys. Rev. D* **44**, 3501–3516 (1991). <https://doi.org/10.1103/PhysRevD.44.3501>
 88. T. Sjöstrand, S. Mrenna, P.Z. Skands, PYTHIA 6.4 physics and manual. *JHEP* **05**, 026 (2006). <https://doi.org/10.1088/1126-6708/2006/05/026>. arXiv:hep-ph/0603175
 89. T. Sjöstrand et al., An introduction to PYTHIA 8.2. *Comput. Phys. Commun.* **191**, 159–177 (2015). <https://doi.org/10.1016/j.cpc.2015.01.024>. arXiv:1410.3012 [hep-ph]
 90. P. Skands, S. Carrazza, J. Rojo, Tuning PYTHIA 8.1: the Monash 2013 Tune. *Eur. Phys. J. C* **74**, 3024 (2014). <https://doi.org/10.1140/epjc/s10052-014-3024-y>. arXiv:1404.5630 [hep-ph]
 91. R. Brun, F. Carminati, S. Gianì, CERNO program library long write-up, W5013 GEANT detector description and simulation tool. Technical Report. CERN-W-5013 (1994). <https://cds.cern.ch/record/1082634>
 92. ALICE Collaboration, S. Acharya et al., Measurement of beauty and charm production in pp collisions at $\sqrt{s} = 5.02$ TeV via non-prompt and prompt D mesons. *JHEP* **05**, 220 (2021). [https://doi.org/10.1007/JHEP05\(2021\)220](https://doi.org/10.1007/JHEP05(2021)220). arXiv:2102.13601 [nucl-ex]
 93. STAR Collaboration, C. Adler et al., Elliptic flow from two and four particle correlations in Au+Au collisions at $\sqrt{s_{NN}} = 130$ GeV. *Phys. Rev. C* **66**, 034904 (2002). <https://doi.org/10.1103/PhysRevC.66.034904>. arXiv:nucl-ex/0206001
 94. I. Selyuzhenkov, S. Voloshin, Effects of non-uniform acceptance in anisotropic flow measurement. *Phys. Rev. C* **77**, 034904 (2008). <https://doi.org/10.1103/PhysRevC.77.034904>. arXiv:0707.4672 [nucl-th]
 95. ALICE Collaboration, S. Acharya et al., Energy dependence and fluctuations of anisotropic flow in Pb–Pb collisions at $\sqrt{s_{NN}} = 5.02$ and 2.76 TeV. *JHEP* **07**, 103 (2018). [https://doi.org/10.1007/JHEP07\(2018\)103](https://doi.org/10.1007/JHEP07(2018)103). arXiv:1804.02944 [nucl-ex]

100. M. Cacciari, M. Greco, P. Nason, The p_T spectrum in heavy flavor hadroproduction. *JHEP* **05**, 007 (1998). <https://doi.org/10.1088/1126-6708/1998/05/007>. arXiv:hep-ph/9803400
101. W. Ke, Y. Xu, S.A. Bass, Linearized Boltzmann–Langevin model for heavy quark transport in hot and dense QCD matter. *Phys. Rev. C* **98**, 064901 (2018). <https://doi.org/10.1103/PhysRevC.98.064901>. arXiv:1806.08848 [nucl-th]
102. M. He, R. Rapp, Hadronization and charm-hadron ratios in heavy-ion collisions. *Phys. Rev. Lett.* **124**, 042301 (2020). <https://doi.org/10.1103/PhysRevLett.124.042301>. arXiv:1905.09216 [nucl-th]
103. S. Cao, T. Luo, G.-Y. Qin, X.-N. Wang, Linearized Boltzmann transport model for jet propagation in the quark-gluon plasma: heavy quark evolution. *Phys. Rev. C* **94**, 014909 (2016). <https://doi.org/10.1103/PhysRevC.94.014909>. arXiv:1605.06447 [nucl-th]
104. S. Li, W. Xiong, R. Wan, Relativistic Langevin dynamics: charm versus beauty. *Eur. Phys. J. C* **80**, 1113 (2020). <https://doi.org/10.1140/epjc/s10052-020-08708-y>. arXiv:2012.02489 [hep-ph]
105. S.-Q. Li et al., Heavy flavor quenching and flow: the roles of initial condition, pre-equilibrium evolution, and in-medium interaction. *Chin. Phys. C* **44**, 114101 (2020). <https://doi.org/10.1088/1674-1137/abadee>. arXiv:2005.03330 [nucl-th]
106. S.-Q. Li et al., Scaling behaviors of heavy flavor meson suppression and flow in different nuclear collision systems at the LHC. *Eur. Phys. J. C* **81**, 1035 (2021). <https://doi.org/10.1140/epjc/s10052-021-09833-y>. arXiv:2108.06648 [hep-ph]
107. W. Ke, Y. Xu, S.A. Bass, Modified Boltzmann approach for modeling the splitting vertices induced by the hot QCD medium in the deep Landau–Pomeranchuk–Migdal region. *Phys. Rev. C* **100**, 064911 (2019). <https://doi.org/10.1103/PhysRevC.100.064911>. arXiv:1810.08177 [nucl-th]
108. Z. Citron et al., Report from Working Group 5: future physics opportunities for high-density QCD at the LHC with heavy-ion and proton beams. CERN Yellow Rep. Monogr. **7**, 1159–1410 (2019). <https://doi.org/10.23731/CYRM-2019-007.1159>. arXiv:1812.06772 [hep-ph]

ALICE Collaboration

S. Acharya¹²⁶, D. Adamová⁸⁶, G. Aglieri Rinella³³, M. Agnello³⁰, N. Agrawal⁵¹, Z. Ahammed¹³⁴, S. Ahmad¹⁶, S. U. Ahn⁷¹, I. Ahuja³⁸, A. Akhmedov¹⁴², M. Al-Turany⁹⁷, D. Aleksandrov¹⁴², B. Alessandro⁵⁶, H. M. Alfanda⁶, R. Alfaro Molina⁶⁷, B. Ali¹⁶, A. Alici²⁶, N. Alizadehvandchali¹¹⁵, A. Alkin³³, J. Alme²¹, G. Alocco⁵², T. Alt⁶⁴, A. R. Altamura⁵⁰, I. Altsybeev⁹⁵, M. N. Anaam⁶, C. Andrei⁴⁶, N. Andreou¹¹⁴, A. Andronic¹³⁷, V. Anguelov⁹⁴, F. Antinori⁵⁴, P. Antonioli⁵¹, N. Apadula⁷⁴, L. Aphecetche¹⁰³, H. Appelshäuser⁶⁴, C. Arata⁷³, S. Arcelli²⁶, M. Aresti²³, R. Arnaldi⁵⁶, J. G. M. C. A. Arneiro¹¹⁰, I. C. Arsene²⁰, M. Arslanodk¹³⁹, A. Augustinus³³, R. Averbeck⁹⁷, M. D. Azmi¹⁶, H. Baba¹²³, A. Badalà⁵³, J. Bae¹⁰⁴, Y. W. Baek⁴¹, X. Bai¹¹⁹, R. Bailhache⁶⁴, Y. Bailung⁴⁸, A. Balbino³⁰, A. Baldisseri¹²⁹, B. Balis², D. Banerjee⁴, Z. Banoo⁹¹, R. Barbera²⁷, F. Barile³², L. Barioglio⁹⁵, M. Barlou⁷⁸, B. Barman⁴², G. G. Barnaföldi¹³⁸, L. S. Barnby⁸⁵, V. Barret¹²⁶, L. Barreto¹¹⁰, C. Bartels¹¹⁸, K. Barth³³, E. Bartsch⁶⁴, N. Bastid¹²⁶, S. Basu⁷⁵, G. Batigne¹⁰³, D. Battistini⁹⁵, B. Batyunya¹⁴³, D. Bauri⁴⁷, J. L. Bazo Alba¹⁰¹, I. G. Bearden⁸³, C. Beattie¹³⁹, P. Becht⁹⁷, D. Behera⁴⁸, I. Belikov¹²⁸, A. D. C. Bell Hechavarria¹³⁷, F. Bellini²⁶, R. Bellwied¹¹⁵, S. Belokurova¹⁴², Y. A. V. Beltran⁴⁵, G. Bencedi¹³⁸, S. Beole²⁵, Y. Berdnikov¹⁴², A. Berdnikova⁹⁴, L. Bergmann⁹⁴, M. G. Besoiu⁶³, L. Betev³³, P. P. Bhaduri¹³⁴, A. Bhasin⁹¹, M. A. Bhat⁴, B. Bhattacharjee⁴², L. Bianchi²⁵, N. Bianchi⁴⁹, J. Bielčik³⁶, J. Bielčiková⁸⁶, J. Biernat¹⁰⁷, A. P. Bigot¹²⁸, A. Bilandzic⁹⁵, G. Biro¹³⁸, S. Biswas⁴, N. Bize¹⁰³, J. T. Blair¹⁰⁸, D. Blau¹⁴², M. B. Blidaru⁹⁷, N. Bluhme³⁹, C. Blume⁶⁴, G. Boca^{22,55}, F. Bock⁸⁷, T. Bodova²¹, A. Bogdanov¹⁴², S. Boi²³, J. Bok⁵⁸, L. Boldizsár¹³⁸, M. Bombara³⁸, P. M. Bond³³, G. Bonomi^{55,133}, H. Borel¹²⁹, A. Borissov¹⁴², A. G. Borquez Carcamo⁹⁴, H. Bossi¹³⁹, E. Botta²⁵, Y. E. M. Bouziani⁶⁴, L. Bratrud⁶⁴, P. Braun-Munzinger⁹⁷, M. Bregant¹¹⁰, M. Broz³⁶, G. E. Bruno^{32,96}, M. D. Buckland²⁴, D. Budnikov¹⁴², H. Buesching⁶⁴, S. Bufalino³⁰, P. Buhler¹⁰², N. Burmasov¹⁴², Z. Buthelezi^{68,122}, A. Bylinkin²¹, S. A. Bysiak¹⁰⁷, M. Cai⁶, H. Caines¹³⁹, A. Caliva²⁹, E. Calvo Villar¹⁰¹, J. M. M. Camacho¹⁰⁹, P. Camerini²⁴, F. D. M. Canedo¹¹⁰, M. Carabas¹²⁵, A. A. Carballo³³, F. Carnesecchi³³, R. Caron¹²⁷, L. A. D. Carvalho¹¹⁰, J. Castillo Castellanos¹²⁹, F. Catalano^{25,33}, C. Ceballos Sanchez¹⁴³, I. Chakaberia⁷⁴, P. Chakraborty⁴⁷, S. Chandra¹³⁴, S. Chapeland³³, M. Chartier¹¹⁸, S. Chattopadhyay¹³⁴, S. Chattopadhyay⁹⁹, T. G. Chavez⁴⁵, T. Cheng^{6,97}, C. Cheshkov¹²⁷, B. Cheynis¹²⁷, V. Chibante Barroso³³, D. D. Chinellato¹¹¹, E. S. Chizzali^{95,a}, J. Cho⁵⁸, S. Cho⁵⁸, P. Chochula³³, D. Choudhury⁴², P. Christakoglou⁸⁴, C. H. Christensen⁸³, P. Christiansen⁷⁵, T. Chujo¹²⁴, M. Ciaccio³⁰, C. Cicalo⁵², F. Cindolo⁵¹, M. R. Ciupek⁹⁷, G. Clai^{51,b}, F. Colamaria⁵⁰, J. S. Colburn¹⁰⁰, D. Colella^{32,96}, M. Colocci²⁶, M. Concas^{33,c}, G. Conesa Balbastre⁷³, Z. Conesa del Valle¹³⁰, G. Contin²⁴, J. G. Contreras³⁶, M. L. Coquet¹²⁹, P. Cortese^{56,132}, M. R. Cosentino¹¹², F. Costa³³, S. Costanza^{22,55}, C. Cot¹³⁰, J. Crkovská⁹⁴, P. Crochet¹²⁶, R. Cruz-Torres⁷⁴, P. Cui⁶, A. Dainese⁵⁴, M. C. Danisch⁹⁴, A. Danu⁶³, P. Das⁸⁰, P. Das⁴, S. Das⁴, A. R. Dash¹³⁷, S. Dash⁴⁷, R. M. H. David⁴⁵, A. De Caro²⁹, G. de Cataldo⁵⁰, J. de Cuveland³⁹, A. De Falco²³, D. De Gruttola²⁹, N. De Marco⁵⁶,

C. De Martin²⁴, S. De Pasquale²⁹, R. Deb¹³³, R. Del Grande⁹⁵, L. Dello Stritto²⁹, W. Deng⁶, P. Dhankher¹⁹, D. Di Bari³², A. Di Mauro³³, B. Diab¹²⁹, R. A. Diaz^{7,143}, T. Dietel¹¹³, Y. Ding⁶, J. Ditzel⁶⁴, R. Divià³³, D. U. Dixit¹⁹, Ø. Djuvsland²¹, U. Dmitrieva¹⁴², A. Dobrin⁶³, B. Dönigus⁶⁴, J. M. Dubinski¹³⁵, A. Dubla⁹⁷, S. Dudi⁹⁰, P. Dupieux¹²⁶, M. Durkac¹⁰⁶, N. Dzalaiova¹³, T. M. Eder¹³⁷, R. J. Ehlers⁷⁴, F. Eisenhut⁶⁴, R. Ejima⁹², D. Elia⁵⁰, B. Erasmus¹⁰³, F. Ercolessi²⁶, F. Erhardt⁸⁹, M. R. Ersdal²¹, B. Espagnon¹³⁰, G. Eulisse³³, D. Evans¹⁰⁰, S. Evdokimov¹⁴², L. Fabbietti⁹⁵, M. Faggin²⁸, J. Faivre⁷³, F. Fan⁶, W. Fan⁷⁴, A. Fantoni⁴⁹, M. Fasel⁸⁷, P. Fedichio³⁰, A. Feliciello⁵⁶, G. Feofilov¹⁴², A. Fernández Téllez⁴⁵, L. Ferrandi¹¹⁰, M. B. Ferrer³³, A. Ferrero¹²⁹, C. Ferrero⁵⁶, A. Ferretti²⁵, V. J. G. Feuillard⁹⁴, V. Filova³⁶, D. Finogeev¹⁴², F. M. Fionda⁵², F. Flor¹¹⁵, A. N. Flores¹⁰⁸, S. Foertsch⁶⁸, I. Fokin⁹⁴, S. Fokin¹⁴², E. Fragiaco⁵⁷, E. Frajna¹³⁸, U. Fuchs³³, N. Funicello²⁹, C. Furget⁷³, A. Furs¹⁴², T. Fusayasu⁹⁸, J. J. Gaardhøje⁸³, M. Gagliardi²⁵, A. M. Gago¹⁰¹, T. Gahlaut⁴⁷, C. D. Galvan¹⁰⁹, D. R. Gangadharan¹¹⁵, P. Ganoti⁷⁸, C. Garabatos⁹⁷, A. T. Garcia¹³⁰, J. R. A. Garcia⁴⁵, E. Garcia-Solis⁹, C. Gargiulo³³, P. Gasik⁹⁷, A. Gautam¹¹⁷, M. B. Gay Ducati⁶⁶, M. Germain¹⁰³, A. Ghimouz¹²⁴, C. Ghosh¹³⁴, M. Giacalone⁵¹, G. Gioachin³⁰, P. Giubellino^{56,97}, P. Giubilato²⁸, A. M. C. Glaenger¹²⁹, P. Glässel⁹⁴, E. Glimos¹²¹, D. J. Q. Goh⁷⁶, V. Gonzalez¹³⁶, M. Gorgon², K. Goswami⁴⁸, S. Gotovac³⁴, V. Grabski⁶⁷, L. K. Graczykowski¹³⁵, E. Grecka⁸⁶, A. Grelli⁵⁹, C. Grigoras³³, V. Grigoriev¹⁴², S. Grigoryan^{1,143}, F. Grosa³³, J. F. Grosse-Oetringhaus³³, R. Grosso⁹⁷, D. Grund³⁶, N. A. Grunwald⁹⁴, G. G. Guardiano¹¹¹, R. Guernane⁷³, M. Guilbaud¹⁰³, K. Gulbrandsen⁸³, T. Gundem⁶⁴, T. Gunji¹²³, W. Guo⁶, A. Gupta⁹¹, R. Gupta⁹¹, R. Gupta⁴⁸, S. P. Guzman⁴⁵, K. Gwizdzial¹³⁵, L. Gyulai¹³⁸, C. Hadjidakis¹³⁰, F. U. Haider⁹¹, S. Haidlova³⁶, H. Hamagaki⁷⁶, A. Hamdi⁷⁴, Y. Han¹⁴⁰, B. G. Hanley¹³⁶, R. Hannigan¹⁰⁸, J. Hansen⁷⁵, M. R. Haque¹³⁵, J. W. Harris¹³⁹, A. Harton⁹, H. Hassan¹¹⁶, D. Hatzifotiadiou⁵¹, P. Hauer⁴³, L. B. Havener¹³⁹, S. T. Heckel⁹⁵, E. Hellbär⁹⁷, H. Helstrup³⁵, M. Hemmer⁶⁴, T. Herman³⁶, G. Herrera Corral⁸, F. Herrmann¹³⁷, S. Herrmann¹²⁷, K. F. Hetland³⁵, B. Heybeck⁶⁴, H. Hillemanns³³, B. Hippolyte¹²⁸, F. W. Hoffmann⁷⁰, B. Hofman⁵⁹, G. H. Hong¹⁴⁰, M. Horst⁹⁵, A. Horzyk², Y. Hou⁶, P. Hristov³³, C. Hughes¹²¹, P. Huhn⁶⁴, L. M. Huhta¹¹⁶, T. J. Humanic⁸⁸, A. Hutson¹¹⁵, D. Hutter³⁹, R. Ilkaev¹⁴², H. Ilyas¹⁴, M. Inaba¹²⁴, G. M. Innocenti³³, M. Ippolitov¹⁴², A. Isakov^{84,86}, T. Isidori¹¹⁷, M. S. Islam⁹⁹, M. Ivanov¹³, M. Ivanov⁹⁷, V. Ivanov¹⁴², K. E. Iversen⁷⁵, M. Jablonski², B. Jacak⁷⁴, N. Jacazio²⁶, P. M. Jacobs⁷⁴, S. Jadlovská¹⁰⁶, J. Jadlovsky¹⁰⁶, S. Jaelani⁸², C. Jahnke¹¹¹, M. J. Jakubowska¹³⁵, M. A. Janik¹³⁵, T. Janson⁷⁰, S. Ji¹⁷, S. Jia¹⁰, A. A. P. Jimenez⁶⁵, F. Jonas⁸⁷, D. M. Jones¹¹⁸, J. M. Jowett^{33,97}, J. Jung⁶⁴, M. Jung⁶⁴, A. Junique³³, A. Jusko¹⁰⁰, M. J. Kabus^{33,135}, J. Kaewjai¹⁰⁵, P. Kalinak⁶⁰, A. S. Kalteyer⁹⁷, A. Kalweit³³, V. Kaplin¹⁴², A. Karasu Uysal⁷², D. Karatovic⁸⁹, O. Karavichev¹⁴², T. Karavicheva¹⁴², P. Karczmarczyk¹³⁵, E. Karpechev¹⁴², U. Keschull⁷⁰, R. Keidel¹⁴¹, D. L. D. Keijdener⁵⁹, M. Keil³³, B. Ketzer⁴³, S. S. Khade⁴⁸, A. M. Khan^{6,119}, S. Khan¹⁶, A. Khanzadeev¹⁴², Y. Kharlov¹⁴², A. Khatun¹¹⁷, A. Khuntia³⁶, B. Kileng³⁵, B. Kim¹⁰⁴, C. Kim¹⁷, D. J. Kim¹¹⁶, E. J. Kim⁶⁹, J. Kim¹⁴⁰, J. S. Kim⁴¹, J. Kim⁵⁸, J. Kim⁶⁹, M. Kim¹⁹, S. Kim¹⁸, T. Kim¹⁴⁰, K. Kimura⁹², S. Kirsch⁶⁴, I. Kisel³⁹, S. Kiselev¹⁴², A. Kisiel¹³⁵, J. P. Kitowski², J. L. Klay⁵, J. Klein³³, S. Klein⁷⁴, C. Klein-Bösing¹³⁷, M. Kleiner⁶⁴, T. Klemenz⁹⁵, A. Kluge³³, A. G. Knospe¹¹⁵, C. Kobdaj¹⁰⁵, T. Kollegger⁹⁷, A. Kondratyev¹⁴³, N. Kondratyeva¹⁴², E. Kondratyuk¹⁴², J. König⁶⁴, S. A. Königstorfer⁹⁵, P. J. Konopka³³, G. Kornakov¹³⁵, S. D. Koryciak², A. Kotliarov⁸⁶, V. Kovalenko¹⁴², M. Kowalski¹⁰⁷, V. Kozuharov³⁷, I. Králik⁶⁰, A. Kravčáková³⁸, L. Krcal^{33,39}, M. Krivda^{60,100}, F. Krizek⁸⁶, K. Krizkova Gajdosova³³, M. Kroesen⁹⁴, M. Krüger⁶⁴, D. M. Krupova³⁶, E. Kryshen¹⁴², V. Kučera⁵⁸, C. Kuhn¹²⁸, P. G. Kuijter⁸⁴, T. Kumaoka¹²⁴, D. Kumar¹³⁴, L. Kumar⁹⁰, N. Kumar⁹⁰, S. Kumar³², S. Kundu³³, P. Kurashvili⁷⁹, A. Kurepin¹⁴², A. B. Kurepin¹⁴², A. Kuryakin¹⁴², S. Kushpil⁸⁶, M. J. Kweon⁵⁸, Y. Kwon¹⁴⁰, S. L. La Pointe³⁹, P. La Rocca²⁷, A. Lakrathok¹⁰⁵, M. Lamanna³³, R. Langoy¹²⁰, P. Lariou³³, E. Laudi³³, L. Lautner^{33,95}, R. Lavička¹⁰², R. Lea^{55,133}, H. Lee¹⁰⁴, I. Legrand⁴⁶, G. Legras¹³⁷, J. Leibrach³⁹, T. M. Lelek², R. C. Lemmon⁸⁵, I. León Monzón¹⁰⁹, M. M. Lesch⁹⁵, E. D. Lesser¹⁹, P. Lévai¹³⁸, X. Li¹⁰, J. Lien¹²⁰, R. Lietava¹⁰⁰, I. Likmeta¹¹⁵, B. Lim²⁵, S. H. Lim¹⁷, V. Lindenstruth³⁹, A. Lindner⁴⁶, C. Lippmann⁹⁷, D. H. Liu⁶, J. Liu¹¹⁸, G. S. S. Liveraro¹¹¹, I. M. Lofnes²¹, C. Loizides⁸⁷, S. Lokos¹⁰⁷, J. Lomker⁵⁹, P. Loncar³⁴, X. Lopez¹²⁶, E. López Torres⁷, P. Lu^{97,119}, J. R. Luhder¹³⁷, M. Lunardon²⁸, G. Luparello⁵⁷, Y. G. Ma⁴⁰, M. Mager³³, A. Maire¹²⁸, M. V. Makariev³⁷, M. Malaev¹⁴², G. Malfattore²⁶, N. M. Malik⁹¹, Q. W. Malik²⁰, S. K. Malik⁹¹, L. Malinina^{143,f}, D. Mallick^{80,130}, N. Mallick⁴⁸, G. Mandaglio^{31,53}, S. K. Mandal⁷⁹, V. Manko¹⁴², F. Manso¹²⁶, V. Manzari⁵⁰, Y. Mao⁶, R. W. Marcjan², G. V. Margagliotti²⁴, A. Margotti⁵¹, A. Marín⁹⁷, C. Markert¹⁰⁸, P. Martinengo³³, M. I. Martínez⁴⁵, G. Martínez García¹⁰³, M. P. P. Martins¹¹⁰, S. Masciocchi⁹⁷

M. Masera²⁵ , A. Masoni⁵² , L. Massacrier¹³⁰ , O. Massen⁵⁹ , A. Mastroserio^{50,131} , O. Matonoha⁷⁵ , S. Mattiazzo²⁸ , A. Matyja¹⁰⁷ , C. Mayer¹⁰⁷ , A. L. Mazuecos³³ , F. Mazzaschi²⁵ , M. Mazzilli³³ , J. E. Mdhului¹²² , Y. Melikyan⁴⁴ , A. Menchaca-Rocha⁶⁷ , E. Meninno^{29,102} , A. S. Menon¹¹⁵ , M. Meres¹³ , S. Mhlanga^{68,113} , Y. Miake¹²⁴ , L. Micheletti³³ , D. L. Mihaylov⁹⁵ , K. Mikhaylov^{142,143} , A. N. Mishra¹³⁸ , D. Miśkowiec⁹⁷ , A. Modak⁴ , B. Mohanty⁸⁰ , M. Mohisin Khan^{16,d} , M. A. Molander⁴⁴ , S. Monira¹³⁵ , C. Mordasini¹¹⁶ , D. A. Moreira De Godoy¹³⁷ , I. Morozov¹⁴² , A. Morsch³³ , T. Mrnjavac³³ , V. Muccifora⁴⁹ , S. Muhuri¹³⁴ , J. D. Mulligan⁷⁴ , A. Mulliri²³ , M. G. Munhoz¹¹⁰ , R. H. Munzer⁶⁴ , H. Murakami¹²³ , S. Murray¹¹³ , L. Musa³³ , J. Musinsky⁶⁰ , J. W. Myrcha¹³⁵ , B. Naik¹²² , A. I. Nambrath¹⁹ , B. K. Nandi⁴⁷ , R. Nania⁵¹ , E. Nappi⁵⁰ , A. F. Nassirpour¹⁸ , A.
Nath⁹⁴ , C. Natrass¹²¹ , M. N. Naydenov³⁷ , A. Neagu²⁰ , A. Negru¹²⁵ , L. Nellen⁶⁵ , R. Nepeivoda⁷⁵ , S. Nese²⁰ , G. Neskovic³⁹ , N. Nicassio⁵⁰ , B. S. Nielsen⁸³ , E. G. Nielsen⁸³ , S. Nikolaev¹⁴² , S. Nikulin¹⁴² , V. Nikulin¹⁴² , F. Noferini⁵¹ , S. Noh¹² , P. Nomokonov¹⁴³ , J. Norman¹¹⁸ , N. Novitzky¹²⁴ , P. Nowakowski¹³⁵ , A. Nyanin¹⁴² , J. Nystrand²¹ , M. Ogino⁷⁶ , S. Oh¹⁸ , A. Ohlson⁷⁵ , V. A. Okorokov¹⁴² , J. Oleniacz¹³⁵ , A. C. Oliveira Da Silva¹²¹ , A. Onnerstad¹¹⁶ , C. Oppedisano⁵⁶ , A. Ortiz Velasquez⁶⁵ , J. Otwinowski¹⁰⁷ , M. Oya⁹² , K. Oyama⁷⁶ , Y. Pachmayer⁹⁴ , S. Padhan⁴⁷ , D. Pagano^{55,133} , G. Paic⁶⁵ , A. Palasciano⁵⁰ , S. Panebianco¹²⁹ , H. Park¹²⁴ , H. Park¹⁰⁴ , J. Park⁵⁸ , J. E. Parkkila³³ , Y. Patley⁴⁷ , R. N. Patra⁹¹ , B. Paul²³ , H. Pei⁶ , T. Peitzmann⁵⁹ , X. Peng¹¹ , M. Pennisi²⁵ , S. Perciballi²⁵

, D. Peresunko¹⁴² , G. M. Perez⁷ , Y. Pestov¹⁴² , V. Petrov¹⁴² , M. Petrovici⁴⁶ , R. P. Pezzi^{66,103} , S. Piano⁵⁷ , M. Pikna¹³ , P. Pillot¹⁰³ , O. Pinazza^{33,51} , L. Pinsky¹¹⁵ , C. Pinto⁹⁵ , S. Pisano⁴⁹ , M. Płoskoń⁷⁴ , M. Planinic⁸⁹ , F. Pliquet⁶⁴ , M. G. Poghosyan⁸⁷ , B. Polichtchouk¹⁴² , S. Politano³⁰ , N. Poljak⁸⁹ , A. Pop⁴⁶ , S. Porteboeuf-Houssais¹²⁶ , V. Pozdniakov¹⁴³ , I. Y. Pozos⁴⁵ , K. K. Pradhan⁴⁸ , S. K. Prasad⁴ , S. Prasad⁴⁸ , R. Preghenella⁵¹ , F. Prino⁵⁶ , C. A. Pruneau¹³⁶ , I. Pshenichnov¹⁴² , M. Puccio³³ , S. Pucillo²⁵ , Z. Pugelova¹⁰⁶ , S. Qiu⁸⁴ , L. Quaglia²⁵ , S. Ragoni¹⁵ , A. Rai¹³⁹ , A. Rakotozafindrabe¹²⁹ , L. Ramello^{56,132} , F. Rami¹²⁸ , S. A. R. Ramirez⁴⁵ , T. A. Rancien⁷³ , M. Rasa²⁷ , S. S. Räsänen⁴⁴ , R. Rath⁵¹ , M. P. Rauch²¹ , I. Ravasenga⁸⁴ , K. F. Read^{87,121} , C. Reckziegel¹¹² , A. R. Redelbach³⁹ , K. Redlich^{79,e} , C. A. Reetz⁹⁷

, A. Rehman²¹ , F. Reidt³³ , H. A. Reme-Ness³⁵ , Z. Rescakova³⁸ , K. Reygers⁹⁴ , A. Riabov¹⁴² , V. Riabov¹⁴² , R. Ricci²⁹ , M. Richter²⁰ , A. A. Riedel⁹⁵ , W. Riegler³³ , A. G. Riffero²⁵ , C. Ristea⁶³ , M. V. Rodriguez³³ , M. Rodríguez Cahuanti⁴⁵ , K. Røed²⁰ , R. Rogalev¹⁴² , E. Rogochaya¹⁴³ , T. S. Rogoschinski⁶⁴ , D. Rohr³³ , D. Röhrich²¹ , P. F. Rojas⁴⁵ , S. Rojas Torres³⁶ , P. S. Rokita¹³⁵ , G. Romanenko²⁶ , F. Ronchetti⁴⁹ , A. Rosano^{31,53} , E. D. Rosas⁶⁵ , K. Roslon¹³⁵ , A. Rossi⁵⁴ , A. Roy⁴⁸ , S. Roy⁴⁷ , N. Rubini²⁶ , O. V. Rueda¹¹⁵ , D. Ruggiano¹³⁵ , R. Rui²⁴ , P. G. Russek² , R. Russo⁸⁴ , A. Rustamov⁸¹ , E. Ryabinkin¹⁴² , Y. Ryabov¹⁴² , A. Rybicki¹⁰⁷ , H. Rytkonen¹¹⁶ , J. Ryu¹⁷ , W. Rzeska¹³⁵ , O. A. M. Saarimaki⁴⁴ , S. Sadhu³² , S. Sadovsky¹⁴² , J. Saetre²¹ , K. Šafařík³⁶ , P. Saha⁴² , S. K. Saha⁴ , S. Saha⁸⁰

, B. Sahoo⁴⁷ , B. Sahoo⁴⁸ , R. Sahoo⁴⁸ , S. Sahoo⁶¹ , D. Sahu⁴⁸ , P. K. Sahu⁶¹ , J. Saini¹³⁴ , K. Sajdakova³⁸ , S. Sakai¹²⁴ , M. P. Salvan⁹⁷ , S. Sambyal⁹¹ , D. Samitz¹⁰² , I. Sanna^{33,95} , T. B. Saramela¹¹⁰ , P. Sarma⁴² , V. Sarritzu²³ , V. M. Sarti⁹⁵ , M. H. P. Sas¹³⁹ , J. Schambach⁸⁷ , H. S. Scheid⁶⁴ , C. Schiaua⁴⁶ , R. Schicker⁹⁴ , A. Schmah⁹⁷ , C. Schmidt⁹⁷ , H. R. Schmidt⁹³ , M. O. Schmidt³³ , M. Schmidt⁹³ , N. V. Schmidt⁸⁷ , A. R. Schmier¹²¹ , R. Schotter¹²⁸ , A. Schröter³⁹ , J. Schukraft³³ , K. Schweda⁹⁷ , G. Scioli²⁶ , E. Scomparin⁵⁶ , J. E. Seger¹⁵ , Y. Sekiguchi¹²³ , D. Sekihata¹²³ , M. Selina⁸⁴ , I. Selyuzhenkov⁹⁷ , S. Senyukov¹²⁸ , J. J. Seo^{58,94} , D. Serebryakov¹⁴² , L. Šerkšnytė⁹⁵ , A. Sevcenco⁶³ , T. J. Shaba⁶⁸ , A. Shabetai¹⁰³ , R. Shahoyan³³ , A. Shangaraev¹⁴² , A. Sharma⁹⁰ , B. Sharma⁹¹ , D. Sharma⁴⁷ , H. Sharma^{54,107}

, M. Sharma⁹¹ , S. Sharma⁷⁶ , S. Sharma⁹¹ , U. Sharma⁹¹ , A. Shatat¹³⁰ , O. Sheibani¹¹⁵ , K. Shigaki⁹² , M. Shimomura⁷⁷ , J. Shin¹² , S. Shirinkin¹⁴² , Q. Shou⁴⁰ , Y. Sibiriyak¹⁴² , S. Siddhanta⁵² , T. Siemiarzucuk⁷⁹ , T. F. Silva¹¹⁰ , D. Silvermyr⁷⁵ , T. Simantathammakul¹⁰⁵ , R. Simeonov³⁷ , B. Singh⁹¹ , B. Singh⁹⁵ , K. Singh⁴⁸ , R. Singh⁸⁰ , R. Singh⁹¹ , R. Singh⁴⁸ , S. Singh¹⁶ , V. K. Singh¹³⁴ , V. Singhal^{134</}

V. V. Torres¹⁰³ , A. G. Torres Ramos³² , A. Trifiró^{31,53} , A. S. Triolo^{31,33,53} , S. Tripathy⁵¹ , T. Tripathy⁴⁷ , S. Trogolo³³ , V. Trubnikov³ , W. H. Trzaska¹¹⁶ , T. P. Trzcinski¹³⁵ , A. Tumkin¹⁴² , R. Turrisi⁵⁴ , T. S. Tvetter²⁰ , K. Ullaland²¹ , B. Ulukutlu⁹⁵ , A. Uras¹²⁷ , G. L. Usai²³ , M. Vala³⁸ , N. Valle²² , L. V. R. van Doremalen⁵⁹ , M. van Leeuwen⁸⁴ , C. A. van Veen⁹⁴ , R. J. G. van Weelden⁸⁴ , P. Vande Vyvre³³ , D. Varga¹³⁸ , Z. Varga¹³⁸ , M. Vasileiou⁷⁸ , A. Vasiliev¹⁴² , O. Vázquez Doce⁴⁹ , V. Vechernin¹⁴² , E. Vercellin²⁵ , S. Vergara Limón⁴⁵ , R. Verma⁴⁷ , L. Vermunt⁹⁷ , R. Vértesi¹³⁸ , M. Verweij⁵⁹ , L. Vickovic³⁴ , Z. Vilakazi¹²² , O. Villalobos Baillie¹⁰⁰ , A. Villani²⁴ , A. Vinogradov¹⁴² , T. Virgili²⁹ , M. M. O. Virta¹¹⁶ , V. Vislavicius⁷⁵ , A. Vodopyanov¹⁴³ , B. Volkel³³ , M. A. Völkl⁹⁴ , K. Voloshin¹⁴² , S. A. Voloshin¹³⁶ , G. Volpe³² , B. von Haller³³ , I. Vorobyev⁹⁵ , N. Vozniuk¹⁴² , J. Vrláková³⁸ , J. Wan⁴⁰ , C. Wang⁴⁰ , D. Wang⁴⁰ , Y. Wang⁴⁰ , Y. Wang⁶ , A. Wegrzynek³³ , F. T. Weiglhofer³⁹ , S. C. Wenzel³³ , J. P. Wessels¹³⁷ , S. L. Weyhmler¹³⁹ , J. Wiechula⁶⁴ , J. Wikne²⁰ , G. Wilk⁷⁹ , J. Wilkinson⁹⁷ , G. A. Willems¹³⁷ , B. Windelband⁹⁴ , M. Winn¹²⁹ , J. R. Wright¹⁰⁸ , W. Wu⁴⁰ , Y. Wu¹¹⁹ , R. Xu⁶ , A. Yadav⁴³ , A. K. Yadav¹³⁴ , S. Yalcin⁷² , Y. Yamaguchi⁹² , S. Yang²¹ , S. Yano⁹² , Z. Yin⁶ , I.-K. Yoo¹⁷ , J. H. Yoon⁵⁸ , H. Yu¹² , S. Yuan²¹ , A. Yuncu⁹⁴ , V. Zaccolo²⁴ , C. Zampolli³³ , F. Zanone⁹⁴ , N. Zardoshti³³ , A. Zarochentsev¹⁴² , P. Závada⁶² , N. Zaviyalov¹⁴² , M. Zhalov¹⁴² , B. Zhang⁶ , C. Zhang¹²⁹ , L. Zhang⁴⁰ , S. Zhang⁴⁰ , X. Zhang⁶ , Y. Zhang¹¹⁹ , Z. Zhang⁶ , M. Zhao¹⁰ , V. Zhrebchevskii¹⁴² , Y. Zhi¹⁰ , D. Zhou⁶ , Y. Zhou⁸³ , J. Zhu^{6,54} , Y. Zhu⁶ , S. C. Zugravel⁵⁶ , N. Zurlo^{55,133}

- ¹ A.I. Alikhanyan National Science Laboratory (Yerevan Physics Institute) Foundation, Yerevan, Armenia
- ² AGH University of Science and Technology, Cracow, Poland
- ³ Bogolyubov Institute for Theoretical Physics, National Academy of Sciences of Ukraine, Kiev, Ukraine
- ⁴ Department of Physics and Centre for Astroparticle Physics and Space Science (CAPSS), Bose Institute, Kolkata, India
- ⁵ California Polytechnic State University, San Luis Obispo, CA, USA
- ⁶ Central China Normal University, Wuhan, China
- ⁷ Centro de Aplicaciones Tecnológicas y Desarrollo Nuclear (CEADEN), Havana, Cuba
- ⁸ Centro de Investigación y de Estudios Avanzados (CINVESTAV), Mexico City and Mérida, Mexico
- ⁹ Chicago State University, Chicago, IL, USA
- ¹⁰ China Institute of Atomic Energy, Beijing, China
- ¹¹ China University of Geosciences, Wuhan, China
- ¹² Chungbuk National University, Cheongju, Republic of Korea
- ¹³ Faculty of Mathematics, Physics and Informatics, Comenius University Bratislava, Bratislava, Slovak Republic
- ¹⁴ COMSATS University Islamabad, Islamabad, Pakistan
- ¹⁵ Creighton University, Omaha, NE, USA
- ¹⁶ Department of Physics, Aligarh Muslim University, Aligarh, India
- ¹⁷ Department of Physics, Pusan National University, Pusan, Republic of Korea
- ¹⁸ Department of Physics, Sejong University, Seoul, Republic of Korea
- ¹⁹ Department of Physics, University of California, Berkeley, CA, USA
- ²⁰ Department of Physics, University of Oslo, Oslo, Norway
- ²¹ Department of Physics and Technology, University of Bergen, Bergen, Norway
- ²² Dipartimento di Fisica, Università di Pavia, Pavia, Italy
- ²³ Dipartimento di Fisica dell'Università and Sezione INFN, Cagliari, Italy
- ²⁴ Dipartimento di Fisica dell'Università and Sezione INFN, Trieste, Italy
- ²⁵ Dipartimento di Fisica dell'Università and Sezione INFN, Turin, Italy
- ²⁶ Dipartimento di Fisica e Astronomia dell'Università and Sezione INFN, Bologna, Italy
- ²⁷ Dipartimento di Fisica e Astronomia dell'Università and Sezione INFN, Catania, Italy
- ²⁸ Dipartimento di Fisica e Astronomia dell'Università and Sezione INFN, Padua, Italy
- ²⁹ Dipartimento di Fisica 'E.R. Caianiello' dell'Università and Gruppo Collegato INFN, Salerno, Italy
- ³⁰ Dipartimento DISAT del Politecnico and Sezione INFN, Turin, Italy
- ³¹ Dipartimento di Scienze MIFT, Università di Messina, Messina, Italy
- ³² Dipartimento Interateneo di Fisica 'M. Merlin' and Sezione INFN, Bari, Italy
- ³³ European Organization for Nuclear Research (CERN), Geneva, Switzerland
- ³⁴ Faculty of Electrical Engineering, Mechanical Engineering and Naval Architecture, University of Split, Split, Croatia
- ³⁵ Faculty of Engineering and Science, Western Norway University of Applied Sciences, Bergen, Norway
- ³⁶ Faculty of Nuclear Sciences and Physical Engineering, Czech Technical University in Prague, Prague, Czech Republic

- 37 Faculty of Physics, Sofia University, Sofia, Bulgaria
- 38 Faculty of Science, P.J. Šafárik University, Kosice, Slovak Republic
- 39 Frankfurt Institute for Advanced Studies, Johann Wolfgang Goethe-Universität Frankfurt, Frankfurt, Germany
- 40 Fudan University, Shanghai, China
- 41 Gangneung-Wonju National University, Gangneung, Republic of Korea
- 42 Department of Physics, Gauhati University, Guwahati, India
- 43 Helmholtz-Institut für Strahlen- und Kernphysik, Rheinische Friedrich-Wilhelms-Universität Bonn, Bonn, Germany
- 44 Helsinki Institute of Physics (HIP), Helsinki, Finland
- 45 High Energy Physics Group, Universidad Autónoma de Puebla, Puebla, Mexico
- 46 Horia Hulubei National Institute of Physics and Nuclear Engineering, Bucharest, Romania
- 47 Indian Institute of Technology Bombay (IIT), Mumbai, India
- 48 Indian Institute of Technology Indore, Indore, India
- 49 INFN, Laboratori Nazionali di Frascati, Frascati, Italy
- 50 INFN, Sezione di Bari, Bari, Italy
- 51 INFN, Sezione di Bologna, Bologna, Italy
- 52 INFN, Sezione di Cagliari, Cagliari, Italy
- 53 INFN, Sezione di Catania, Catania, Italy
- 54 INFN, Sezione di Padova, Padova, Italy
- 55 INFN, Sezione di Pavia, Pavia, Italy
- 56 INFN, Sezione di Torino, Turin, Italy
- 57 INFN, Sezione di Trieste, Trieste, Italy
- 58 Inha University, Incheon, Republic of Korea
- 59 Institute for Gravitational and Subatomic Physics (GRASP), Utrecht University/Nikhef, Utrecht, The Netherlands
- 60 Institute of Experimental Physics, Slovak Academy of Sciences, Kosice, Slovak Republic
- 61 Institute of Physics, Homi Bhabha National Institute, Bhubaneswar, India
- 62 Institute of Physics of the Czech Academy of Sciences, Prague, Czech Republic
- 63 Institute of Space Science (ISS), Bucharest, Romania
- 64 Institut für Kernphysik, Johann Wolfgang Goethe-Universität Frankfurt, Frankfurt, Germany
- 65 Instituto de Ciencias Nucleares, Universidad Nacional Autónoma de México, Mexico City, Mexico
- 66 Instituto de Física, Universidade Federal do Rio Grande do Sul (UFRGS), Porto Alegre, Brazil
- 67 Instituto de Física, Universidad Nacional Autónoma de México, Mexico City, Mexico
- 68 iThemba LABS, National Research Foundation, Somerset West, South Africa
- 69 Jeonbuk National University, Jeonju, Republic of Korea
- 70 Johann-Wolfgang-Goethe Universität Frankfurt Institut für Informatik, Fachbereich Informatik und Mathematik, Frankfurt, Germany
- 71 Korea Institute of Science and Technology Information, Daejeon, Republic of Korea
- 72 KTO Karatay University, Konya, Turkey
- 73 Laboratoire de Physique Subatomique et de Cosmologie, Université Grenoble-Alpes, CNRS-IN2P3, Grenoble, France
- 74 Lawrence Berkeley National Laboratory, Berkeley, CA, USA
- 75 Division of Particle Physics, Department of Physics, Lund University, Lund, Sweden
- 76 Nagasaki Institute of Applied Science, Nagasaki, Japan
- 77 Nara Women's University (NWU), Nara, Japan
- 78 Department of Physics, School of Science, National and Kapodistrian University of Athens, Athens, Greece
- 79 National Centre for Nuclear Research, Warsaw, Poland
- 80 National Institute of Science Education and Research, Homi Bhabha National Institute, Jatni, India
- 81 National Nuclear Research Center, Baku, Azerbaijan
- 82 National Research and Innovation Agency-BRIN, Jakarta, Indonesia
- 83 Niels Bohr Institute, University of Copenhagen, Copenhagen, Denmark
- 84 Nikhef, National Institute for Subatomic Physics, Amsterdam, The Netherlands
- 85 Nuclear Physics Group, STFC Daresbury Laboratory, Daresbury, UK
- 86 Nuclear Physics Institute of the Czech Academy of Sciences, Husinec-Řež, Czech Republic
- 87 Oak Ridge National Laboratory, Oak Ridge, TN, USA
- 88 Ohio State University, Columbus, OH, USA

- 89 Physics Department, Faculty of Science, University of Zagreb, Zagreb, Croatia
- 90 Physics Department, Panjab University, Chandigarh, India
- 91 Physics Department, University of Jammu, Jammu, India
- 92 Physics Program and International Institute for Sustainability with Knotted Chiral Meta Matter (SKCM2), Hiroshima University, Hiroshima, Japan
- 93 Physikalisches Institut, Eberhard-Karls-Universität Tübingen, Tübingen, Germany
- 94 Physikalisches Institut, Ruprecht-Karls-Universität Heidelberg, Heidelberg, Germany
- 95 Physik Department, Technische Universität München, Munich, Germany
- 96 Politecnico di Bari and Sezione INFN, Bari, Italy
- 97 Research Division and ExtreMe Matter Institute EMMI, GSI Helmholtzzentrum für Schwerionenforschung GmbH, Darmstadt, Germany
- 98 Saga University, Saga, Japan
- 99 Saha Institute of Nuclear Physics, Homi Bhabha National Institute, Kolkata, India
- 100 School of Physics and Astronomy, University of Birmingham, Birmingham, UK
- 101 Sección Física, Departamento de Ciencias, Pontificia Universidad Católica del Perú, Lima, Peru
- 102 Stefan Meyer Institut für Subatomare Physik (SMI), Vienna, Austria
- 103 SUBATECH, IMT Atlantique, Nantes Université, CNRS-IN2P3, Nantes, France
- 104 Sungkyunkwan University, Suwon City, Republic of Korea
- 105 Suranaree University of Technology, Nakhon Ratchasima, Thailand
- 106 Technical University of Košice, Kosice, Slovak Republic
- 107 The Henryk Niewodniczanski Institute of Nuclear Physics, Polish Academy of Sciences, Cracow, Poland
- 108 The University of Texas at Austin, Austin, TX, USA
- 109 Universidad Autónoma de Sinaloa, Culiacán, Mexico
- 110 Universidade de São Paulo (USP), São Paulo, Brazil
- 111 Universidade Estadual de Campinas (UNICAMP), Campinas, Brazil
- 112 Universidade Federal do ABC, Santo André, Brazil
- 113 University of Cape Town, Cape Town, South Africa
- 114 University of Derby, Derby, UK
- 115 University of Houston, Houston, TX, USA
- 116 University of Jyväskylä, Jyväskylä, Finland
- 117 University of Kansas, Lawrence, KS, USA
- 118 University of Liverpool, Liverpool, UK
- 119 University of Science and Technology of China, Hefei, China
- 120 University of South-Eastern Norway, Kongsberg, Norway
- 121 University of Tennessee, Knoxville, TN, USA
- 122 University of the Witwatersrand, Johannesburg, South Africa
- 123 University of Tokyo, Tokyo, Japan
- 124 University of Tsukuba, Tsukuba, Japan
- 125 University Politehnica of Bucharest, Bucharest, Romania
- 126 Université Clermont Auvergne, CNRS/IN2P3, LPC, Clermont-Ferrand, France
- 127 Institut de Physique des 2 Infinis de Lyon, Université de Lyon, CNRS/IN2P3, Lyon, France
- 128 Université de Strasbourg, CNRS, IPHC UMR 7178, 67000 Strasbourg, France
- 129 Département de Physique Nucléaire (DPhN), Université Paris-Saclay, Centre d'Etudes de Saclay (CEA), IRFU, Saclay, France
- 130 Université Paris-Saclay, CNRS/IN2P3, IJCLab, Orsay, France
- 131 Università degli Studi di Foggia, Foggia, Italy
- 132 Università del Piemonte Orientale, Vercelli, Italy
- 133 Università di Brescia, Brescia, Italy
- 134 Variable Energy Cyclotron Centre, Homi Bhabha National Institute, Kolkata, India
- 135 Warsaw University of Technology, Warsaw, Poland
- 136 Wayne State University, Detroit, MI, USA
- 137 Institut für Kernphysik, Westfälische Wilhelms-Universität Münster, Münster, Germany
- 138 Wigner Research Centre for Physics, Budapest, Hungary

¹³⁹ Yale University, New Haven, CT, USA

¹⁴⁰ Yonsei University, Seoul, Republic of Korea

¹⁴¹ Zentrum für Technologie und Transfer (ZTT), Worms, Germany

¹⁴² Affiliated with an Institute Covered by a Cooperation Agreement with CERN, Geneva, Switzerland

¹⁴³ Affiliated with an International Laboratory Covered by a Cooperation Agreement with CERN, Geneva, Switzerland

^a Also at: Max-Planck-Institut für Physik, Munich, Germany

^b Also at: Italian National Agency for New Technologies, Energy and Sustainable Economic Development (ENEA), Bologna, Italy

^c Also at: Dipartimento DET del Politecnico di Torino, Turin, Italy

^d Also at: Department of Applied Physics, Aligarh Muslim University, Aligarh, India

^e Also at: Institute of Theoretical Physics, University of Wrocław, Wrocław, Poland

^f Also at: An Institution Covered by a Cooperation Agreement with CERN, Geneva, Switzerland